Regularised direct inversion to compaction in the Groningen reservoir using measurements from optical leveling campaigns

S.M. Bierman, F. Kraaijeveld, S.J. Bourne

Datum   November 2015

Editors   Jan van Elk & Dirk Doornhof

General Introduction

A statistical methodology is presented for estimation of reservoir compaction in the Groningen gas reservoir through direct inversion using subsidence measurements from optical leveling campaigns. With this methodology estimates of compaction can be obtained without reliance on certain assumptions, in particular:

- There is no need to assume a functional form for the relationship between reservoir compressibility and porosity.
- There is no need to assume a functional form for the relationship between reservoir compaction and pore pressure decline.

The main disadvantage of the proposed methodology is that the independent contribution of compaction in different reservoir sections to the observed subsidence bowl cannot be estimated without imposing some form of regularisation. The minimum lateral resolution at which the independent contribution of neighbouring section in the reservoir can be estimated is about the burial depth of the reservoir, which is about 3 kilometers for the Groningen reservoir.

Results indicate that the spatio-temporal progression of the subsidence bowl above the Groningen reservoir can be described well by a set of compaction estimates which vary smoothly in both time and space. This means that, for a given epoch, differences in compaction estimates between neighbouring blocks in the reservoir were restricted to be small. Estimates of compaction correlated strongly with pore pressure decline.

It is concluded that direct inversion to compaction from subsidence as measured in optical leveling campaigns provides a useful methodology to estimate reservoir compaction above producing gas fields.

Title	Regularised direct inversion to compaction in the Groningen reservoir using measurements from optical leveling campaigns		Date	November 2015
			Initiator	NAM
Author(s)	S.M. Bierman, F. Kraaijeveld, S.J. Bourne	Editors	Jan van Elk Dirk Doornhof	
Organisation	Shell	Organisation	NAM	
Place in the Study and Data Acquisition Plan	Study Theme: Deformation Model Comment: An alternative technique was developed to estimate reservoir compaction from subsidence measurements.			
Directliy linked research	(1) Seismological Modelling (2) Hazard Assessment			
Used data	Optical leveling campaigns from 1964-2013			
Associated organisation	Shell			
Assurance	Internal Assurance only.			

Regularised direct inversion to compaction in the Groningen reservoir using measurements from optical leveling campaigns

Regularised direct inversion to compaction in the Groningen reservoir using measurements from optical leveling campaigns

by

S.M. Bierman (GSNL-PTD/TASE), F. Kraaijeveld (GSNL-PTI/RC), S.J. Bourne (GSNL-PTI/RC)

Shell Global Solutions International B.V., Amsterdam

Further electronic copies can be obtained from the Global Information Centre.

Executive Summary

Statistical methodology is presented that may be used to estimate reservoir compaction through direct inversion using subsidence measurements from optical leveling campaigns. The main motivation for choosing this methodology was that models currently in use by the Nederlandse Aardolie Maatschappij (NAM) produce biased estimates of the subsidence bowl as evidenced by the existence of spatio-temporal patterns in the residuals of these models, indicating that these models are likely misspecified and/or that model input such as rock porosity maps or pressure grids are biased. Direct inversion to compaction provides a useful alternative view on the available information because estimates of compaction can be obtained without reliance on certain assumptions that are made in the current models, in particular:

- There is no need to assume a functional form for the relationship between reservoir compactibility and rock porosity.
- There is no need to assume that the rock porosity per reservoir section is known.
- There is no need to assume a functional form for the relationship between reservoir compaction and pore pressure decline.

The main disadvantage of the proposed methodology is that the independent contribution of compaction in different reservoir sections to the observed subsidence bowl cannot be estimated with sufficient precision without imposing regularisation. The lateral resolution of reservoir compaction obtained by inversion of surface displacement data is limited to about the burial depth of the reservoir, which is almost 3 kilometers. Regularisation is achieved by imposing spatial smoothness on the compaction estimates and by restricting estimates to be non-negative (i.e. only decreases in volume are allowed in the reservoir). The degree of spatial smoothness is estimated by penalising differences between compaction estimates in neighbouring reservoir sections, and the penalty which is given to the differences in estimates is estimated through a spatial cross-validation scheme (CV-scheme). The regularisation methodology was effective in enabling the estimation of spatially resolved compaction estimates without over-fitting of the optical leveling measurements. The spatio-temporal progression of the subsidence bowl could be described well by a spatio-temporally smooth set of compaction estimates. For all reservoir resolutions and CV-schemes, estimates of compaction correlated strongly with pore pressure decline. A basic ('first-order') forward simulation model was defined with constant rates of compaction per unit of pore pressure decline per aggregated reservoir section. This first-order forward model performed well in comparison with the current models in use by NAM in its ability to explain the variation in subsidence measurements. Our results indicate that direct inversion to compaction from subsidence as measured in optical leveling campaigns provides a useful alternative methodology to estimate reservoir compaction because certain key assumptions that are made in the current models in use by NAM can be relaxed. At a second modeling stage, the apparent existence (or absence) of relationships between estimates of reservoir compaction and variables such as reservoir pressures, thickness or rock porosity can be investigated. In this report, the investigation of such relationships has been restricted to a basic ('first-order') model assuming constant rates of compaction per unit pore pressure decline per reservoir section, but a wider variety of models needs to be investigated.

Amsterdam, May 2015.

Table of Contents

List of Figures

List of Tables

1. Introduction

The load of the sediments above the gas bearing Rotliegend sandstone formation of the Groningen gas field is supported partially by the rock matrix itself and partially by the pressurized fluid and gas within the pore space of the rock. The decrease in fluid volume in the rock associated with gas extraction results in pore volume reduction (compaction) at the reservoir level. The compaction of the reservoir results in a measurable amount of subsidence at the surface, and likely induces fault slip. NAM is required to forecast subsidence above the Groningen gas field on the basis of scenarios for gas extraction. Spatially resolved estimates of compaction rates are also necessary for seismic hazard models in which the seismicity is estimated as a fraction of the volumetric strain due to compaction.

Reservoir compaction may in principle be measured *in situ* through the use of radio-active bullets. NAM has several of these bullets in place, but the quality and spatial coverage are insufficient to estimate spatio-temporal trends in reservoir compaction. Compaction is modelled as a function of pressure depletion, the compressibility of the rock and the thickness of the reservoir. A number of rock physics models are currently in use by NAM: a linear, bi-linear, time-decay and Isotach model (NAM [2013]). These models are calibrated using subsidence measurements such as from optical leveling campaigns. Forecasts of the shape and maximum depth of the subsidence bowl differ substantially between these models. Laboratory compaction measurements of core samples of the Rotliegend sandstone are available, but these data unfortunately cannot be used to determine with confidence whether strain is linearly or non-linearly related to pore pressure. Subsidence rates as measured at a benchmark near the centre of the Groningen field in relation to rates of pore pressure decline (Figure 4.9 in NAM [2013]) were better described by a bi-linear model, with a change in the subsidence per unit of pore pressure decline when pressures are reduced to below a certain level. Such bi-linearity has also been observed in other fields (Ameland and Roswinkel) and these observations were at the basis of the introduction of the bi-linear compaction model which was the preferred compaction model at NAM until 2011. More recently, for the Ameland gas field it was observed that decreasing gas depletion rates were not followed directly by decreasing subsidence rates. This observation of delayed compressibility led to the development of the time decay model in which a time-delayed response of compaction to pore pressure decline at start-up is assumed (Mossop et al. [2011]). In all current NAM models the uni-axial compaction coefficient of a reservoir section is estimated as a function of the porosity of the rock in that section. The relationship between compaction coefficients and porosity differs between the models, and is based on trend lines fitted to laboratory measurements on cores taken from the reservoir (technical addendum to the winningsplan Groningen 2013). The laboratory data indicate that uni-axial compaction coefficients tend to increase with increasing porosity. However, uni-axial compaction coefficients can only be estimated with low precision on the basis of porosity measurements, and the laboratory measurements might not be representative for overburden compressibility.

The current level of understanding of the rock physics of the Groningen field is insufficient to confidently identify a single subsidence model, nor to eliminate any of the current models as possible candidates. The motivation for introducing the bi-linear and time-decay models was based to a large extent on a comparison of predicted and observed subsidence rates at a few of the available measurement locations. A more formal methodology is lacking for comparing the (relative) performance of the different models in terms of how well they are able to explain the spatio-temporal variation in measured subsidence rates at all measurement locations.

In this report, we:

- Describe the results of an assessment of the (relative) ability of models currently in use by NAM to explain the spatio-temporal variation in subsidence rates as measured during optical leveling surveys. Satellite interferometric SAR (InSAR) measurements were available as well, but we limited ourselves to optical leveling surveys because improvements to the methodology for processing of the InSAR data were ongoing at the time of writing this report.

- Describe statistical methodology that can be used for estimating compaction based on direct inversion from optical leveling. In the proposed methodology, in contrast to the existing NAM models, it is not necessary to assume a functional form for the relationship between pressure decline and compaction, nor to explicitly describe the spatial variation in compaction coefficients as a function of spatial variation in rock porosity. Direct inversion to compaction provides a useful alternative view on the available information because estimates of compaction can be obtained without reliance on certain assumptions that are made in the current models, in particular:

  - There is no a-priori assumed functional form for the relationship between reservoir compactibility and rock porosity.

  - A spatially resolved map with estimates of rock porosity per reservoir section is not required as model input.

  - There is no a-priori assumed functional relationship between reservoir compaction and pore pressure decline.

  - Estimates of compaction can be obtained without assuming that the spatial variation in the thickness of the reservoir is known.

Once space-time series of estimates of reservoir compaction have been obtained, the existence of relationships and the functional form thereof between compaction estimates and pore pressure decline, thickness of the reservoir and rock porosity can be investigated.

2. Subsidence measurements from Optical Leveling surveys

2.1. Introduction

Subsidence (vertical displacements) at the surface has been monitored using optical leveling techniques since 1964 (at the onset of gas production from the Groningen field) and, more recently, using satellite interferometric SAR (InSAR) and Global Positioning Systems (GPS). Optical leveling surveys provide measurements of relative height differences between benchmarks for pairs of measurement campaigns (epochs). Leveling measurement campaigns for the Groningen field have been held at approximately five-year intervals (ranging from 1 to 8 years), with the last campaign in 2013. The number and spatial coverage of benchmarks differs greatly between campaigns (Figure 2.1), resulting in a wide variation in available benchmarks between epochs. A higher temporal and spatial coverage can be achieved with InSAR compared to leveling surveys. There is thus a clear advantage in using both leveling and InSAR data. However, as a first step this initial report focuses on a new methodology for inverting the leveling data. At the time of writing this report a new methodology for the processing of the InSAR data was being developed.
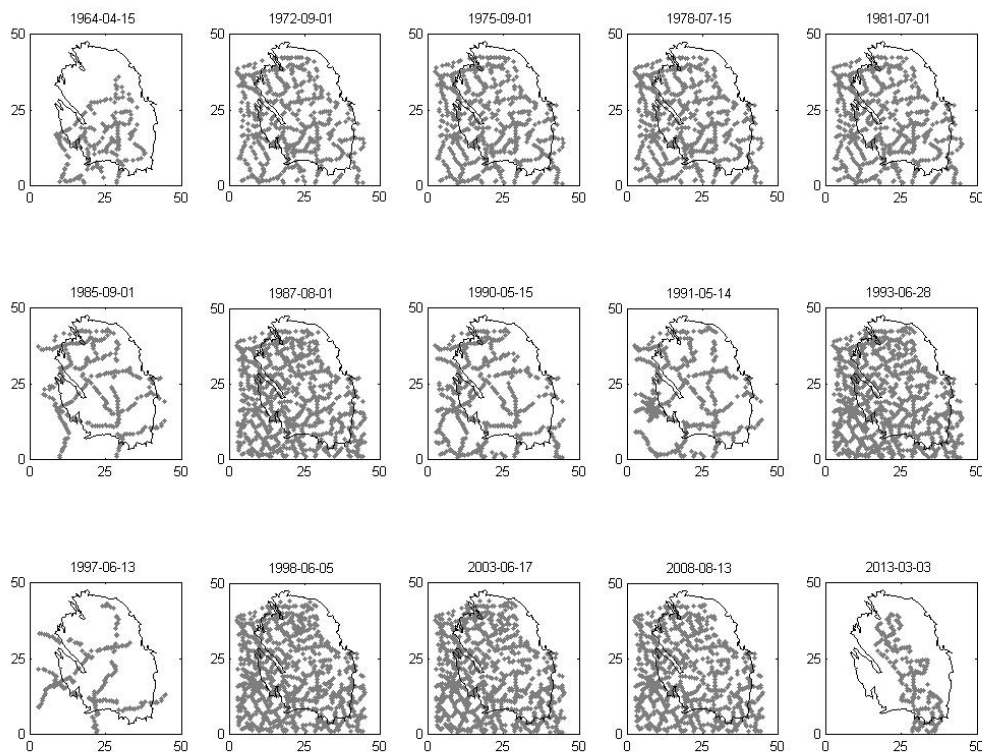
Figure 2.1.: Locations of benchmarks of the optical leveling campaigns.

2.2. Double differencing

For each epoch (combination of measurement campaigns, with the epoch defined by the beginning- and end-date of each pair of campaigns), the change between the two campaigns in the measured height differences between benchmarks can be used as a measure of subsidence. This means that the leveling data needs to be "double-differenced", by:

1. Spatial differencing: within each campaign express the measured height of each benchmark as relative to the height of one of the benchmarks.

2. Temporal differencing: take the difference between two campaigns of the measured relative height differences between benchmarks.

It is important to note that in order to be able to compare predicted and observed subsidence, both model predictions and measurements need to be double-differenced with respect to the same spatial and temporal reference points. The optical leveling data as provided by NAM is in the form of height differences between benchmarks expressed relative to the same benchmark for each leveling campaign (Figure 2.2). We note that in this report we have used the Rijksdriehoek (RD) geographical referencing frame to produce maps but subtracted a value of 200000 from the eastings and a value of 240000 from the northings of the RD grid. The geographical location of the reference benchmark in RD coordinates is: Easting=249080 and Northing=554740.
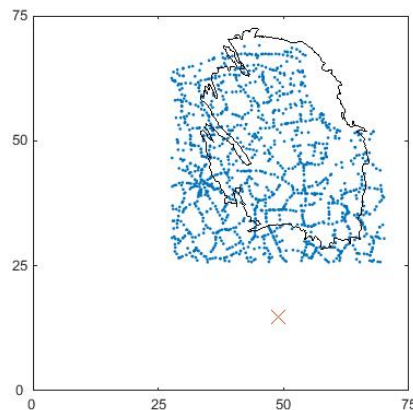
Figure 2.2.: The location of the reference benchmark (indicated by x) used for spatial differencing for all epochs. Note that we have used the Rijksdriehoek (RD) geographical referencing frame but in this map (and in other maps in this report) subtracted a value of 200000 from the eastings and a value of 240000 from the northings of the RD grid. The geographical location of the reference benchmark in RD coordinates is: Easting=249080 and Northing=554740. The units of the tick labels are in kilometers.

3. Assessment of the ability of NAM models to explain the variation in optical leveling measurements

3.1. Introduction

Discrepancies between predicted and measured subsidence may arise from any or a combination of:

1. Deviations due to errors in measurements and processes other than compaction:

   a) Errors in measurements. Relative height differences between benchmarks are measured with error. These measurement errors, as well as the processing of the measurements (e.g. reference of all heights to the height of a common benchmark and data reconciliation to "close" loops of benchmarks) are known to lead to spatial patterns (spatial covariance structures) in errors.

   b) Subsidence caused by processes other than reservoir compaction. For subsidence may be caused by salt mining activities, or benchmarks located on dikes may subside due to changes in the level of water saturation of sediments or salt mining. Ignoring the subsidence caused by such other processes will lead to both spatial and temporal patterns (spatio-temporal covariance structures) in errors (and therefore also in residuals). Subsidence caused by processes other than reservoir compaction is thought to take place on smaller spatial length scales than the smooth subsidence bowl caused by reservoir compaction.

2. Model misspecifications. One or more processes may be missing from the NAM models, or functional relationships in the models may have been misspecified. For example, the geomechanical Green's function or the assumed relationship between porosity and uni-axial compaction coefficients may be misspecified.

3. Errors in model input. The input to the NAM models are subject to uncertainty and may be biased. For example, the current NAM models assume that the pressure grids, porosity grid and spatial extent of the reservoir are unbiased and known without error.

4. Model calibration errors.

   a) Measurements from the leveling survey are not spread evenly in time and space. If this is not taken into account in the calibration of the model (for example when ordinary least squares fitting is used), and when there are discrepancies between the predicted and measured changes in the subsidence bowl, the extent to which such discrepancies play a role in the sums of squares is determined by the (arbitrary) spread of measurements in time and space. Ordinary least squares methodology is currently used for calibrating the NAM models.

   b) All data points have been assigned equal weight in the calibration of the models.

   c) Inconsistent double-differencing of model output and leveling data.

3.2. Matching predictions to observations

The predictions from the NAM models were made available on a 500 by 500 meter grid on the first of January of each calendar year. In order to match the model predictions with measurements from the optical leveling surveys, temporal interpolation was applied to compute model output at the dates of the surveys, and each benchmark was assigned the predicted value in the grid cell nearest to that benchmark (nearest neighbour assignment).

It is important to note that the height differences between benchmarks as predicted by the NAM models have not been expressed as height differences relative to the same reference benchmark as was used in the leveling data for spatial differencing. It was not possible to check the predicted time-trends in the amount of subsidence at this reference benchmark because the spatial extent of the provided grids did include the reference benchmark location. Visualisations of the subsidence bowls as predicted by the NAM models indicate that only small amounts of subsidence are predicted at the reference benchmark, and that any bias introduced by the inconsistency in double-differencing (see section 2.2) between the model predictions and the leveling data are likely to be small. Nevertheless, we recommend that in future both model calibration and assessment of model fit to the data model predictions and measurements are double-differenced in exactly the same way.

3.3. Results

We have used the following conventions:

1. Positive numbers indicate subsidence, whereas negative numbers indicate upheave. For example, a measured subsidence of +2cm between two leveling campaigns at benchmark A indicates that this benchmark has been measured to be 2 cm lower relative to the reference benchmark in the last campaign compared to the first campaign.

2. Residuals in this report are defined as the difference between the measured subsidence and the predicted subsidence. For example, a residual of -2cm at a benchmark indicates that the model predicted more subsidence than was measured (over-prediction). In contrast, a residual of +2cm at a benchmark indicates that the model predicted less subsidence than was measured (under-prediction).

While all leveling survey measurements have been spatially differenced with respect to the same reference benchmark, many different possible choices remain for temporal differencing. The ability of the models to predict long-term changes in the shape of the subsidence bowl may be investigated by differencing the leveling campaigns of 2008 and 1972, which both had a relatively good spatial coverage of benchmarks (Figure 2.1). All models exhibit a similar ability to predict the changes in the subsidence bowl over this time period (Figure 3.1), and exhibit a similar spatial pattern in residuals with a tendency to over-predict subsidence in the northern part of the field and under-predict in the southern part of the field (Figure 3.2).

All NAM models have epochs during which they either systematically under-predict or over-predict subsidence in either all or part of the subsidence bowl, for example for the 1972-09-01 - 1975-09-01 epoch (Figure A.2), the 1987-08-01 - 1993-06-08 epoch (Figure A.3) or the 2003-06-17 - 2008-08-13 epoch (Figure A.4).

3.4. Summary and conclusions

1. All models have a similar ability to predict long-term changes in the shape of the subsidence bowl (Figure 3.1). For long-term predictions, all models exhibit a similar spatio-temporal
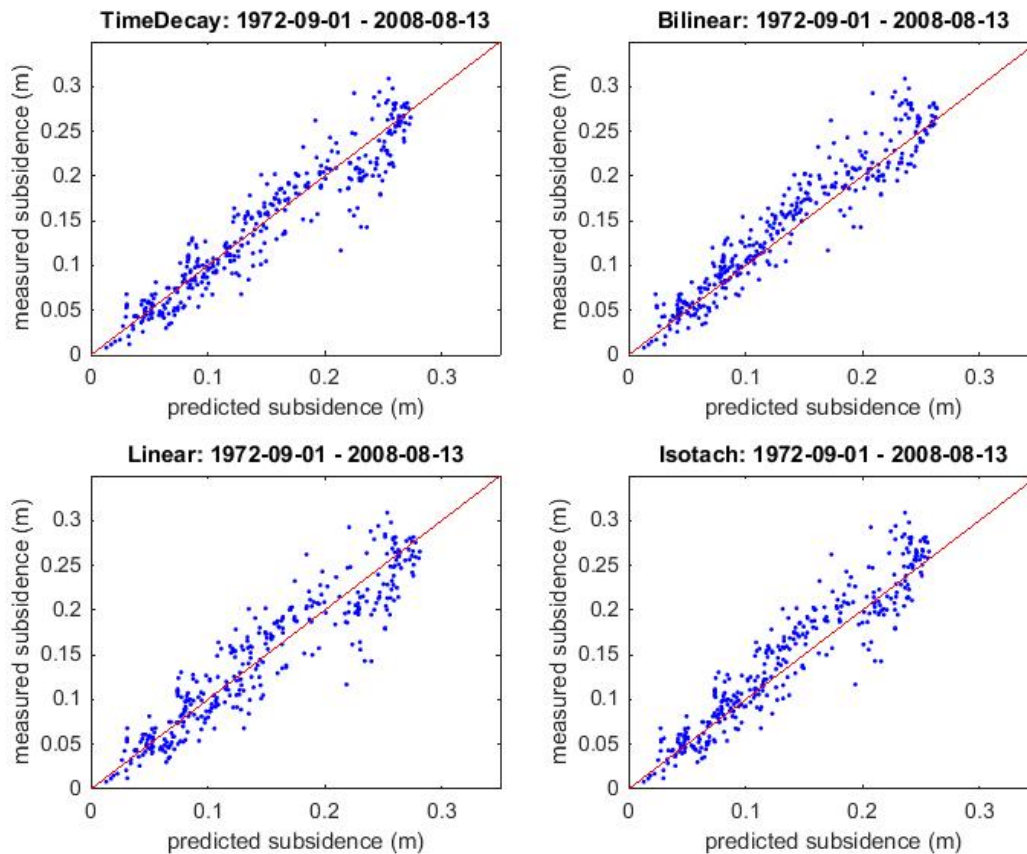
Figure 3.1.: Predicted versus measured subsidence for all NAM models for the 1972-09-01 - 2008-08-13 epoch.

pattern in residuals with a tendency to over-predict subsidence in the northern part of the field and under-predict in the southern part of the field (Figure 3.2).

2. All models have periods during which they either systematically under-predict or over-predict subsidence in either all or part of the space (Figure A.2, A.3, A.4).

3. The use of ordinary least squares methods for model calibration may lead to biased parameter estimates due to the uneven spread of measurements from the leveling survey in time and space in combination with the spatio-temporal patterns in residuals.

4. Discrepancies between predicted and measured subsidence may arise for a number of reasons, as listed in section 3.1. The spatio-temporal patterns in residuals are pronounced and may indicate that the models have in some way been mis-specified. However, subsidence may be caused by processes other than reservoir compaction, and measurement error and the processing of measurements may induce spatio-temporal covariances in errors. In addition, model inputs such as pressure grids may be subject to errors.

5. There is no evidence that any one of the current models has better predictive capabilities than the others.

3.5. Recommendations

1. The height differences between benchmarks as predicted by the NAM models have not been expressed as height differences relative to the same reference benchmark as was used in the leveling data for spatial differencing. Although any biases that may be introduced by this are likely to be small, we recommend that an alternative model calibration workflow is set up in which model predictions and measurements are double-differenced in exactly the same way. In addition, we recommend that different spatial reference benchmarks are used for spatial differencing for each of the epochs used for model calibration.

2. Graphs which are used to visualise the ability of models to explain the time-trends in subsidence at only one or a few of the measurement locations are uninformative. Instead, the relative ability of models to explain both long-term and short-term changes in the shape of the subsidence bowl should be assessed by plotting model predictions against all measurements for a number of epochs, including spatial plots of model residuals.

3. In order to obtain a better quantitative understanding of the size and structure of errors in model input, we recommend that reservoir engineers are asked to provide a range of pressure grids which reflect the uncertainty in these grids. Predictions for all models should be generated for each of these grids.

4. We recommend that in the model calibration workflow the patterns in model residuals are formally accommodated by the estimation of random effects (variance components) for spatial blocks, epochs and combinations of spatial blocks and epochs. This will lead to more realistic estimates of standard errors of parameters.

5. Correlations in measurement error may play a role and this also deserves further investigation.
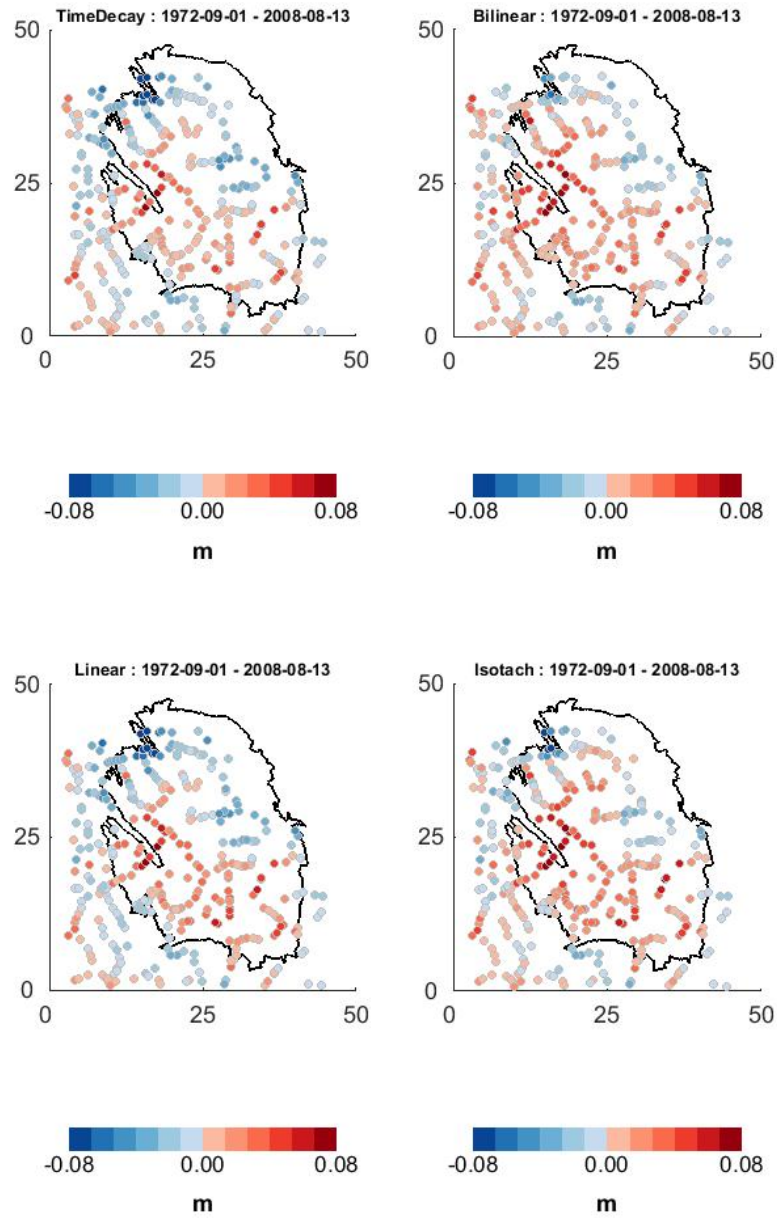
Figure 3.2.: Spatial maps of residuals (predicted - measured subsidence) for the NAM models for the 1972-09-01 - 2008-08-13 epoch.

4. Direct inversion to reservoir compaction

4.1. Motivation

The spatio-temporal patterns in residuals of the NAM models may indicate that these models are misspecified and/or suffer from biased model input. It was therefore decided to try to derive estimates of reservoir compaction through direct inversion to compaction from the optical leveling campaigns (see e.g. Muntendam-Bos et al. [2008]). Here, we define compaction as bulk reservoir volume change per unit area. With such a direct inversion to compaction some assumptions that are made in the NAM models can be relaxed or more closely investigated. In particular, estimates of compaction can be obtained without reliance on the following assumptions:

- There is no need to assume a functional form for the relationship between reservoir compressibility and rock porosity.

- There is no need to assume that the rock porosity per reservoir section is known.

- There is no need to assume a functional form for the relationship between reservoir compaction and pore pressure decline.

The main disadvantages of the proposed methodology are:

- The independent contribution of compaction in different reservoir sections to the observed subsidence bowl cannot be estimated with sufficient precision without imposing regularisation. The lateral resolution of reservoir compaction obtained by inversion of surface displacement data is limited to about the burial depth of the reservoir, which is almost 3 kilometers.

- Spatial variation in measurements of vertical displacements unrelated to reservoir compaction with a spatial (lateral) correlation lengths larger than about 3 kilometers will be attributed at least partly if not wholly to reservoir compaction.

The inferred space-time series of compaction can be modelled at a second stage as a function of pore pressure decline, porosity and thickness of the reservoir. A disadvantage of this approach is that all .

Below we describe how to derive estimates of compaction through regularised direct inversion to compaction using subsidence measurements from optical leveling campaigns. Once a spatially resolved series of estimates of compaction has been obtained for a number of epochs, it will be possible to evaluate whether and how these estimates relate to other relevant information such as pore pressure decline and rock porosity.

4.2. Inversion model

Let $\mathbf{Y}_{t_1}$ be the $[k_{t_1} \times 1]$ column vector of measured relative heights of the k_{t_1} benchmarks in the first optical leveling campaign (1964-05-15), $\mathbf{Y}_{t_2}$ the $[k_{t_2} \times 1]$ column vector of measured relative heights in the second campaign (1972-09-01), etc. up to $\mathbf{Y}_{\mathbf{t_{15}}}$ for the most recent campaign (2013-03-03) (see figure 2.1) In this report, by convention, the last element in each column vector $\mathbf{Y}_t$ refers to the relative height of the reference benchmark (figure 2.2) which is zero by definition ($Y_{k_t,t} = 0$). The $[k_{t_2-t_1} \times 1]$ column vector of measurements $\dot{\mathbf{Y}}_{t_2-t_1}$ of subsidence which has

occurred during the epoch $t_2 - t_1$, where $k_{t_2-t_1}$ is the number of benchmarks which were visited in both campaigns, is given by:

$$\dot{\mathbf{Y}}_{t_2-t_1} = \mathbf{Y}_{t_2} - \mathbf{Y}_{t_1} \tag{4.1}$$

We refer to $\dot{\mathbf{Y}}_{t_2-t_1}$ as a vector of double-differenced measurements of subsidence because it is computed by both spatial (with respect to the reference benchmark) and temporal differencing of height measurements from the optical leveling campaigns.

Let $\mathbf{X}$ be the $[k \times n]$ matrix of influence coefficients where $X_{j,i}$ quantifies the amount of vertical displacement at a leveling survey benchmark location j ($j = 1, 2, ..., k$) due to a given amount of compaction in reservoir section i ($i = 1, 2, ..., n$). In this report, by convention, the kth row in matrix $\mathbf{X}$ contains the influence coefficients of each of the n reservoir sections on the location of the reference benchmark. The spatially differenced influence matrix $\dot{\mathbf{X}}$, in which influence coefficients for all benchmarks are expressed as relative to the influence coefficients of the reference benchmark, is given by:

$$\dot{\mathbf{X}} = \mathbf{HX} \tag{4.2}$$

where $\mathbf{H}$ is a $[k \times k]$ difference matrix with a value of 1 on the diagonal except for the combination of the kth row and k^{th} column, a value of -1 in the kth column for all rows except the kth row, and 0 elsewhere (see for example . An example of the For example, for $k = 4$:

Figure 4.1.: Example of the spatial differencing matrix $\mathbf{H}$ (equation 4.2) for $k = 4$ benchmarks.

$$\mathbf{H} = \begin{bmatrix} 1 & 0 & 0 & -1 \\ 0 & 1 & 0 & -1 \\ 0 & 0 & 1 & -1 \\ 0 & 0 & 0 & 0 \end{bmatrix} \tag{4.3}$$

A general model for the vector of double-differenced measurements of subsidence $\dot{\mathbf{Y}}_{t_2-t_1}$ is given by:

$$\dot{\mathbf{Y}}_{t_2-t_1} = \dot{\mathbf{X}}_{t_2-t_1} \mathbf{L}_{t_2-t_1} + \mathbf{E} \tag{4.4}$$

where $\mathbf{L}_{t_2-t_1}$ is a $[n \times 1]$ column vector of compaction in all reservoir blocks during the $t_2 - t_1$ epoch, and $\mathbf{E} \sim \text{MVN}(0, W)$ is a $[k_{t_2-t_1} \times 1]$ column vector of residuals (deviations between predicted and measured subsidence) whose distribution is assumed to be multivariate normal (MVN) with mean zero and $[k_{t_2-t_1} \times k_{t_2-t_1}]$ variance-covariance matrix W. The $[k_{t_2-t_1} \times n]$ matrix $\dot{\mathbf{X}}_{t_2-t_1}$ is obtained by selecting the rows from the $[k \times n]$ matrix $\dot{\mathbf{X}}$ which refer to the benchmarks that were visited in both optical leveling campaigns.

We note that the height measurements of the optical leveling campaigns may be expressed relative to the height of any one of the benchmarks, and a different reference benchmark may be chosen for each campaign. Similarly, it is also possible to choose multiple reference benchmarks and express height measurements of individual bechmarks as relative to one of each of the set of reference benchmarks. The spatial differencing matrix $\mathbf{H}$ needs to be adopted to match the chosen configuration of reference benchmarks and care needs to be taken that the same spatial differencing operation is applied to both the set of measurements and the matrix of influence coefficients. In this report, we have chosen to use a simple set-up with a single reference benchmark which is used for all campaigns (figure 2.2).

For the inverse modeling, we use an analytical solution for displacements at the reservoir level assuming a linear elastic homogeneous halfspace. Within Shell several such analytical solutions

are used, most notably the Geertsma model of a disk-shaped reservoir (Geertsma and Opstal [1973]). More recently, a general analytical solution for displacements due to cuboidal (block-shaped) inclusions with uniform strains has become available (Kuvshinov [2008]), where each reservoir section is a block and is characterized by the coordinates of the 8 vertices of that block $(\vec{r}_b^i = x_{b_{min}}^i, x_{b_{max}}^i, y_{b_{min}}^i, y_{b_{max}}^i, z_{b_{min}}^i, z_{b_{max}}^i)$. In this report, equation 26 in Kuvshinov [2008] has been used to calculate the amount of vertical displacement $X_{j,i}$ at a leveling survey benchmark location with coordinates $\vec{r}_s^j = (x_s^j, y_s^j, z_s^j))$ for a given amount of compaction in reservoir section i:

$$X_{j,i} = \frac{1}{4\pi} \sum_{vertices} \sigma \left\{ F(x_b^i - x_s^j, y_b^i - y_s^j, z_b^i, R) + (3 - 4\nu)F(x_b^i - x_s^j, y_b^i - y_s^j, z_b^i, R) \right\} \tag{4.5}$$

Where ν is a parameter representing the poisson's ratio, σ a summation sign as given in table 4.1, and $F(x, y, z, R)$ and

$$F(x, y, z, R) = z \arctan\left(\frac{xy}{zR}\right) - x \ln|R + y| - y \ln|R + x| \tag{4.6}$$

and

$$R = \sqrt{(x_b - x_s)^2 + (y_b - y_s)^2 + z_b^2}. \tag{4.7}$$

By convention, the vertical coordinate z is directed downwards, and $z = 0$ for an observation point at the surface.

Table 4.1.: Summation sign σ for each of the 8 vertices of a block $(\vec{r}_b^i)$ as used in equation 4.5

x	y	z	σ
min	min	top	-1
max	min	top	1
min	max	top	1
max	max	top	-1
min	min	bottom	1
max	min	bottom	-1
min	max	bottom	-1
max	max	bottom	1

For the current NAM models, a grid of $n = 5813$ blocks of 500x500 meters in width (but with varying thickness and depth) is used to represent the Groningen reservoir. At this resolution, the numbers of parameters to be estimated (the $[n \times 1]$ column matrix **L** in equation 4.4) are large in comparison to the number of optical leveling benchmarks. In addition, it will not be possible to determine the independent contribution of neighbouring blocks in the reservoir to the subsidence bowl because the influences of neighbouring blocks on the benchmark locations (columns in matrix **X**) are very similar. It is therefore not possible to obtain estimates for the compaction for each of the $n = 5813$ blocks without imposing some form of regularisation to decrease the effective number of free parameters (Zhdanov [2002]). Regularisation has been imposed by a combination of the following:

- Reducing the number of parameters to be estimated by creating $n_a < n$ reservoir sections as aggregates of the n 500x500 blocks. The aggregated sections are created by assigning small blocks to larger quadrants based on whether or not the geographical center-points of

the small blocks are contained within the larger quadrants (this is further described in section 4.5).

- Restricting vertical displacements of reservoir blocks to be positive (i.e. allowing for compaction only).
- Penalising first-order spatial differences between estimates of compaction in aggregated reservoir sections. The larger the penalty on spatial differences the more the estimates of compaction in reservoir sections are restricted to vary smoothly over space.

Let $q = 1, 2, ..., n_a$ be an indicator for the aggregated reservoir section q. The $[k \times n_a]$ influence matrix $\dot{\mathbf{X}}^{\mathbf{a}}$ for the aggregated sections is given by:

$$\dot{X}^a_{q,j} = \Sigma^n_{i=1} \left\{ \dot{X}_{i,j} I_{q(i)} \right\}, \tag{4.8}$$

where $I_{q(i)}$ is an indicator function with $I_{q(i)} = 1$ if reservoir block i is part of the aggregated section q and $I_{q(i)} = 0$ otherwise.

We note that for notational convenience from here onwards we have dropped the subscript to identify the epoch. The $[n_a \times 1]$ column vector of compaction of the aggregated reservoir sections $\mathbf{L}^{\mathbf{a}}$ can then be estimated by minimising the sums of squares Q (see e.g. Eilers and Marx [2010]):

$$Q = \left\| \dot{\mathbf{Y}} - \dot{\mathbf{X}}^{\mathbf{a}} \mathbf{L}^{\mathbf{a}} \right\|^2 + \lambda \left\| \mathbf{D} \mathbf{L}^{\mathbf{a}} \right\|^2, \, for L^a_q \geq 0, \tag{4.9}$$

where $\mathbf{D}$ is a $[n_a \times n_a]$ first-order spatial penalty matrix with on the diagonal minus the number of neighbours in the Queen neighbourhood of each of the aggregated reservoir sections, a value of 1 for each of the off-diagonal elements for combinations of sections which are part of the same rook neighbourhood and a value of 0 for all other off-diagonal elements (figure 4.3 and 4.2, see e.g. Besag et al. [1991] or Earnest et al. [2007] for examples of spatial neighbourhoods and their use in regularisation). The regularising coefficient parameter λ governs the penalty which is put on differences between estimates of compaction in reservoir sections which are part of the same neighbourhood. Note that here we have assumed that the errors $\mathbf{E}$ in equation 4.4 are independent and identically distributed. The validity of this assumption will have to be assessed by graphical exploration of the model residuals.
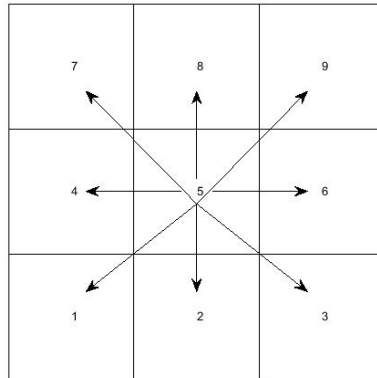
Figure 4.2.: Illustration of a Queen's neighbourhood, which was used for defining the first order spatial penalty matrix $\mathbf{D}$ (equation 4.9). The spatial penalty matrix for this grid of 9 quadrants is illustrated in figure 4.3

Figure 4.3.: Example of a spatial penalty matrix **D** (equation 4.9) for the grid of 9 quadrants as illustrated in figure 4.2

$$\mathbf{D} = \begin{bmatrix} -3 & 1 & 0 & 1 & 1 & 0 & 0 & 0 & 0 \\ 1 & -5 & 1 & 1 & 1 & 1 & 0 & 0 & 0 \\ 0 & 1 & -2 & 0 & 0 & 1 & 0 & 0 & 0 \\ 1 & 1 & 0 & -5 & 1 & 0 & 1 & 1 & 0 \\ 1 & 1 & 1 & 1 & -8 & 1 & 1 & 1 & 1 \\ 0 & 1 & 1 & 0 & 1 & -5 & 0 & 1 & 1 \\ 0 & 0 & 0 & 1 & 1 & 0 & -3 & 1 & 0 \\ 0 & 0 & 0 & 1 & 1 & 1 & 1 & -5 & 1 \\ 0 & 0 & 0 & 0 & 1 & 1 & 0 & 1 & -3 \end{bmatrix} \tag{4.10}$$

4.3. Choice of cross-validation scheme, model complexity and the Bias-Variance trade-off

The penalty term λ in equation 4.9 is estimated using cross-validation (CV, see e.g. G.H. Golub [1979] or Eilers and Marx [2010]), by recursively estimating the parameter column vector $\hat{\mathbf{L}}$ using a subset of all the available benchmark locations and evaluating a measure of fit of the subsidence as predicted by the resulting model to the benchmark locations which had been omitted from the data set. The following steps describe the algorithm which was used for cross-validation:

1. Partition the available set of benchmark locations into a number m of mutually exclusive groups. In practice, we have used two types of cross-validation schemes (CV-schemes), with $m = 4$ and $m = 9$ in which a coarse grid (with either 4 or 9 quadrants) was overlaid over the landscape and each of the benchmarks was allocated to whichever quadrant of this grid it fell into (figure 4.5). We refer to these two CV-schemes as the 4-fold CV-scheme and the 9-fold CV-scheme.

2. For each of the m groups of benchmark locations, and for each of a range of values for λ on a log-linear scale, for example for $\lambda = 10^{0.5}, 10^{0.6}, 10^{0.7}, ..., 10^{2.5}$ do the following:

   a) Split the data set $\dot{\mathbf{Y}}$ into a $[(k - k_m) \times 1]$ training data set $\dot{\mathbf{Y}}_{\mathbf{m,training}}$ and a $[k_m \times 1]$ test data set $\dot{\mathbf{Y}}_{\mathbf{m,test}}$.

   b) Split the influence matrix $\dot{\mathbf{X}}^{\mathbf{a}}$ into a $[(k - k_m) \times n_a]$ training data set $\dot{\mathbf{X}}^{\mathbf{a}}_{\mathbf{m,training}}$ and a $[k_m \times n_a]$ test data set $\dot{\mathbf{X}}^{\mathbf{a}}_{\mathbf{m,test}}$.

   c) Estimate the $[n_A \times 1]$ parameter column vector $\mathbf{L}^a_m$ which minimises the sums of squares $Q = \left\| \dot{\mathbf{Y}}_{\mathbf{m,training}} - \dot{\mathbf{X}}^{\mathbf{a}}_{\mathbf{m,training}} \mathbf{L}^{\mathbf{a}}_{\mathbf{m}} \right\|^2 + \lambda \left\| \mathbf{DL}^{\mathbf{a}}_{\mathbf{m}} \right\|^2$ ($L^a_q \geq 0$). In practice this is done using a data augmentation approach in combination with the *lsqnonneg* optimiser in *matlab* for non-negative least-squares optimisation.

   d) Compute the sums of squares of the differences between predicted and measured subsidence at the test set of benchmark locations $S_m = \left\| \dot{\mathbf{X}}^{\mathbf{a}}_{\mathbf{m,test}} \hat{\mathbf{L}}^{\mathbf{a}}_{\mathbf{m}} - \dot{\mathbf{Y}}_{\mathbf{m,test}} \right\|^2$.

3. Evaluate for which value $\lambda = \lambda_{optim}$ the sums of squares of the differences between predicted and measured subsidence at all of the test sets of benchmark locations combined $S_{tot} = \Sigma_m S_m$ is minimised.

4. Compute the final set of estimates of reservoir compaction $\hat{\mathbf{L}}^a$ by minimising $Q = \left\| \dot{\mathbf{Y}} - \dot{\mathbf{X}}^{\mathbf{a}}\mathbf{L}^{\mathbf{a}} \right\|^2 + \lambda_{optim} \|\mathbf{D}\mathbf{L}^{\mathbf{a}}\|^2$ $(L_q^a \geq 0)$.

The penalty term λ governs how much differences in estimates of reservoir compaction in neighbourhoods of reservoir sections contribute to the overall sum of squares Q in equation 4.9. Larger values of λ will result in a higher degree of spatial smoothness (*stiffness*) in the set of compaction estimates $\hat{\mathbf{L}}^{\mathbf{a}}$. Because of the addition of the penalty term in equation 4.9 estimates of reservoir compaction will inevitably be biased. An increase in the number of reservoir sections n_a may result in a more complex model since the potential number of parameters increases in the $[n_a \times 1]$ vector $\hat{\mathbf{L}}^{\mathbf{a}}$ allowing for more local structure (steeper spatial gradients in compaction estimates) to be inferred. Estimates of compaction will suffer from high variance as the number of reservoir sections (n_a) in the model increases, and introducing some bias in our estimates $\hat{\mathbf{L}}^{\mathbf{a}}$ might lead to a substantial increase in the precision with which these estimates can be made and hence to a substantial increase in the predictive capabilities of the model. The concept of the bias-variance trade-off is illustrated in figure 4.4 (see also e.g. Hastie et al. [2009]). The higher the chosen spatial resolution at the reservoir level, the larger the dimensions of the $[n_a \times n_a]$ matrix D will become relative to the dimensions of the set of measurements Y, and therefore the larger the potential relative contribution of the penalty term to the total sums of squares. By choosing a coarse-grained spatial cross-validation scheme we favour models which are able to predict the overall shape of the subsidence bowl reasonably well. Potential curvature in the subsidence bowl as suggested by the leveling measurements with a spatial signal which is local relative to the grid size of the CV-scheme will not, or only to a small extent, lead to local curvature in the compaction estimates. Because regularisation is imposed by spatial smoothing, estimates of reservoir compaction for sections near and in particular on the edge of the grid will be less well constrained than estimates further away from the edges of the grid. Estimates of compaction in sections on or near the edge of the grid can therefore be expected to have higher variance relative to the estimates in the other reservoir sections.

4.4. Forward model for compaction as a function of pore pressure decline

Once a spatially resolved series of estimates of compaction has been obtained for a number of epochs, it will be possible to evaluate whether and how these estimates relate to other relevant information such as pore pressure decline and rock porosity.

Here, we have explored a first-order model for the relationship between compaction estimates and pore pressure decline with constant rates of compaction per unit of pore pressure decline per aggregated reservoir section. Let $\hat{\mathbf{L}}_{\mathbf{q}}$ be the $[T \times 1]$column vector of estimated compaction in the aggregated reservoir section q for each of T epochs, and $\mathbf{P}_q$ the $[T \times 1]$ column vector of pore pressure declines in aggregated section q. Then, an estimate $\hat{\beta}_q$ of the rate of compaction per unit pore pressure decline is given by linear regression through the origin:

$$\hat{\beta}_q = (\mathbf{P}'_q\mathbf{P}_q)^{-1}\mathbf{P}'_q\hat{\mathbf{L}}_{\mathbf{q}} \tag{4.11}$$

A forward simulation model for reservoir compaction and subsidence was defined based on the first-order model with constant rates of compaction per unit of pore pressure decline per aggregated reservoir section. The subsidence as predicted by this forward model was compared to observations from the optical leveling surveys.

4.5. General description of the workflow

The regularised inversion has been set up as a series of computer scripts in the *matlab* language. A general outline of the workflow is as follows:
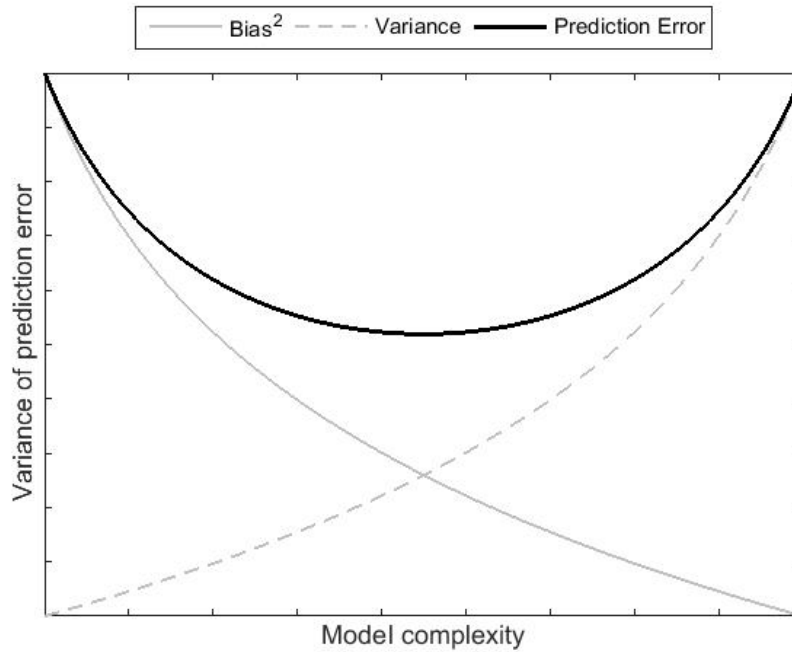
Figure 4.4.: Illustration of the concept of the bias-variance trade-off. A bias-variance trade-off is made in the regularised inversion by imposing spatial smoothness on the compaction estimates, and is mediated by the parameter λ in equation 4.9 which is estimated via spatial cross-validation to evaluate the prediction error of models with increasing complexity.

1. Importing the reservoir data

    a) The geometry of the reservoir: geographical centre-points of the $n = 5813$ blocks of 500x500 meter in width in the reservoir; the top of each block (meters subsurface) and the thickness of each block (meters).

    b) The $[n \times n]$ grids of reservoir pressures for each of a number of dates (typically the first of January of each year for a number of consecutive years).

2. Importing the optical leveling data. Double-differencing and interpolation of pressures to dates of measurement campaigns.

3. Subsetting of benchmarks for use in the inversion. Only benchmarks directly above or just beyond the boundaries of the Groningen gas field were used. The reason for 'clipping' the available set of benchmarks was that subsidence at the western edge of the Groningen field may be caused partly by reservoir compaction in a neighbouring field, whereas subsidence at the southern edge of the field may be partly caused by salt-mining activity.

4. Compute the $[k \times n]$ matrix $\mathbf{X}$ of influence coefficients (equation 4.5). This is done using the $\vec{r}_b^i = x_{b_{min}}^i, x_{b_{max}}^i, y_{b_{min}}^i, y_{b_{max}}^i, z_{b_{min}}^i, z_{b_{max}}^i$ for each block i, using the x and y locations of the vertices, and setting $z_{b_{max}}^i$ equal to the top of the block and $z_{b_{min}}^i$ equal to the top of the block minus 100 meters.

5. Define n_a aggregates of original blocks of 500x500 m in width. This was done as follows:

    a) A coarse grid was overlaid over the landscape with the desired resolution, for example a grid with quadrants of 2500x2500 meters in width.
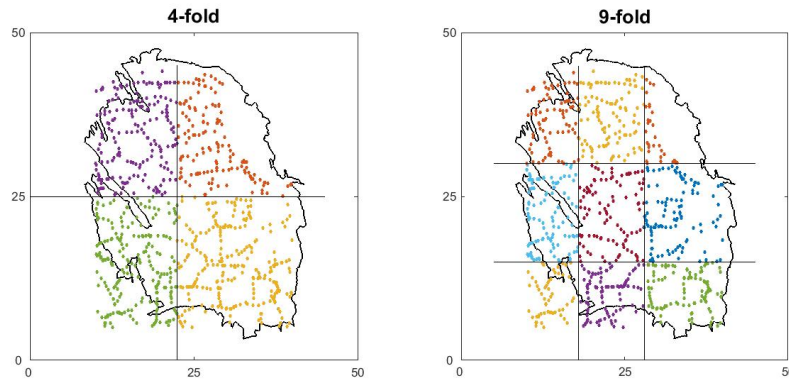
Figure 4.5.: The two spatial cross-validation schemes (CV-schemes) that were used ot estimate the spatial smoothness penalty λ. The space was divided up into four or nine sections each of which were in turn left out of the training data set used for estimation of the compaction estimates, and subsequently used as a test data set to evaluate the predictive capabilities of the resulting model. We refer to these two CV-schemes as the 4-fold CV-scheme and the 9-fold CV-scheme (see text for further explanation).

b) All 500x500 blocks whose geographical center-points fall into the coarse quadrants were aggregated into one larger section.

c) In the case of a coarse grid with quadrants of 2500x2500 meters in width, most aggregated sections will consist of 25 500x500 meter blocks. However, at the edges of the reservoir, there will be quadrants with fewer original blocks. The user is required to specify the minimum number of blocks N_{min} which an aggregated reservoir section is required to contain. In case an aggregate section consists of fewer than N_{min} 500x500 meter blocks, this section is joined to the nearest section.

d) Per aggregate section, we keep track of the number of 500x500 meter blocks this contains, the average pore pressure decline and the average thickness.

e) Compute the aggregated $[k \times n_a]$ influence matrix X^a using equation 4.8.

6. Regularised inversion Step 1: Crossvalidation to determine the optimum penalty λ_{optim}:

a) Specify the T combinations of measurement campaigns which are to be used for temporal differencing. A $[n_a \times 1]$ column vector of estimates of compaction $\hat{\mathbf{L}}$ is made independently for each of the epoch combinations.

b) Specify the range of values for λ for which to do the inversion and evaluate the lack-of-fit criterion using cross-validation.

c) Specify the cross-validation scheme: either a four-fold $m = 4$ or 9-fold $m = 9$ cross-validation scheme in which the landscape is partitioned into respectively 4 or 9 roughly equal-sized quadrants to allocate benchmarks to groups for use in cross-validation.

d) λ_{optim} is chosen as the value which minimises the specified lack-of-fit criterion $\Sigma_m S_m$ summed across all combinations of epochs. When more than one epoch is selected for
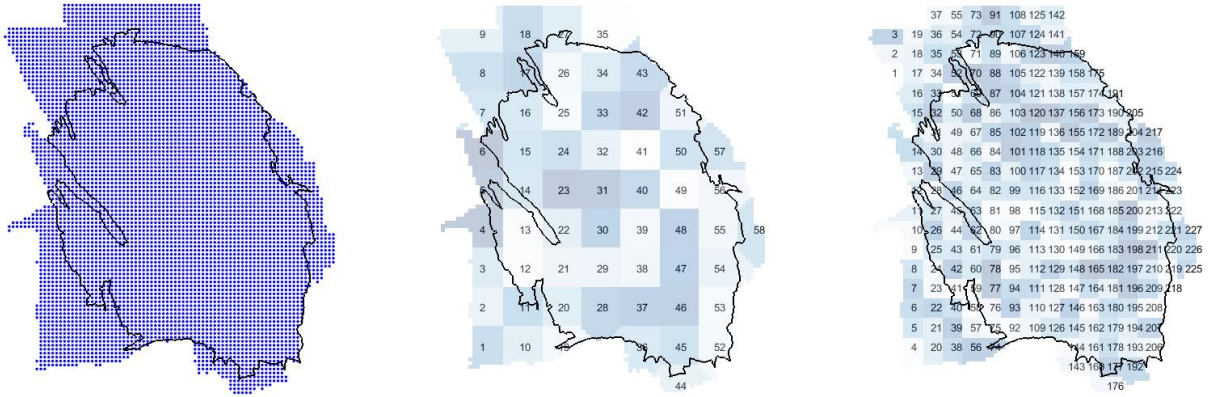
Figure 4.6.: Visualisations of the Groningen reservoir grid at a 500x500 meter resolution
($n = 5813$), and the two spatial resolutions (5kmx5km with $n_a = 58$, and 2.5kmx2.5km
with $n_a = 227$) at which compaction estimates were obtained and reported in this report.
Note that the colors are only included for ease of visual interpretation, and that the num-
bers in the reservoir sections are used as labels in this report to identify individual reser-
voir sections. A larger version of the map of the 2.5km reservoir resolution is given in fig-
ure D.1

use in the inversion, only one value of λ_{optim} is chosen. The penalty on spatial rough-
ness is therefore assumed equal for all epochs.

7. Regularised inversion Step 2:

   a) Use λ_{optim} to estimate a final set of of estimates $\hat{\mathbf{L}}$ for each of the epochs.

   b) Plot predicted versus observed subsidence and plot maps of model residuals. Deter-
   mine whether there is a need to redo the inversion with the exclusion of obvious out-
   liers.

   c) Plot spatial maps of estimated compaction, and store the results.

8. Interpretation of results

   a) Evaluate the relationship between pore pressure decline and estimated compaction per
   aggregated reservoir section. This is done both graphically and formally by estimating
   a first-order model with a constant rate of compaction per unit of pore pressure de-
   cline per aggregated reservoir section. In case several combinations of measurement
   campaigns are used for the inversion there will be more than one estimate of com-
   paction for each aggregated reservoir section. Let $\hat{\mathbf{L}}_{\mathbf{q}}$ be the $[T \times 1]$column vector of
   estimated compaction in the aggregated reservoir section q for each of T epochs, and
   $\mathbf{P}_q$ the $[T \times 1]$ column vector of pore pressure declines in aggregated section q. Esti-
   mate the average rate of compaction per unit pore pressure decline using equation 4.11.

b) Establish a forward simulation model for reservoir compaction and subsidence based on the first-order model with constant rates of compaction per unit of pore pressure decline per aggregated reservoir section. Compare the predicted subsidence with observations from the optical leveling surveys.

5. Results of direct inversion to reservoir compaction

5.1. Introduction

Here we present results for the regularised inversion to reservoir compaction for:

- Aggregated reservoir sections at a 2.5km x 2.5km spatial resolution. Sections were restricted to have a minimum of at least 15 500mx500m blocks; sections with fewer than 15 500mx500m blocks were joined to a neighbouring section (see figure 4.6 and table 5.1).
- Aggregated reservoir sections at a 5km x 5km spatial resolution. Sections were restricted to have a minimum of at least 50 500mx500m blocks; sections with fewer than 50 500mx500m blocks were joined to a neighbouring section (see figure 4.6 and table 5.1).
- For combinations of measurement campaigns (epochs) as depicted in table 5.1.
- Inversions were done for both reservoir resolutions (2.5km and 5km) with a 4-fold and 9-fold CV-schemes (see figure 4.5) for estimation of the optimum penalty λ_{optim}.
- We have used a value of $\nu = 0.25$ for the poisson's ratio to compute the influence matrix $\mathbf{X}$.

Table 5.1.: Epochs (pairs of optical leveling campaigns) used for the regularised inversions to compaction.

epoch start-date (t_1)	epoch end-date (t_2)	number of benchmarks $(k_{t_2-t_1})$
1972-09-01	1975-09-01	381
1972-09-01	1978-07-15	348
1972-09-01	1981-07-01	335
1972-09-01	1987-08-01	310
1972-09-01	1993-06-28	292
1972-09-01	2003-06-17	252
1972-09-01	2008-08-13	240

5.2. Optimum penalties on spatial roughness and inversion results

The variance of the prediction error S_{tot} for a range of increasing values for penalties λ are depicted in figure 5.1 for both reservoir resolutions (2.5km and 5km) and cross-validation schemes (4-fold and 9-fold). The optimal penalties λ_{optim} are given in table 5.2. The optimum penalties are higher for the 2.5km reservoir resolution compared to the 5km reservoir resolution, and higher for the 4-fold CV-scheme compared to the 9-fold CV-scheme. The fit of the models using the optimal penalty to the data is very similar between the four combinations of reservoir resolutions and cross-validation schemes: the root-mean-square error (RMSE) of the fitted model RMSE $= \sqrt{S}$ where $S_{\lambda_{optim}} = \left\| \mathbf{X^a \hat{L}^a_{\lambda_{optim}}} - \mathbf{Y} \right\|^2$ for the 1972-09-01 - 2008-08-13 epoch (RMSE1 in table 5.2) vary between 0.009 m and 0.012 m. The RMSE of the predictions of the first-order forward model based on constant rates of compaction per unit of pore pressure decline (equation 4.11) are also highly similar between the four models, for example for the 1972-09-01 - 2008-08-13 epoch (RMSE2 in table 5.2) and the 1972-09-01 - 2013-03-03 epoch (RMSE3 in table 5.2) the RMSE values vary between 0.012 m - 0.017 m.
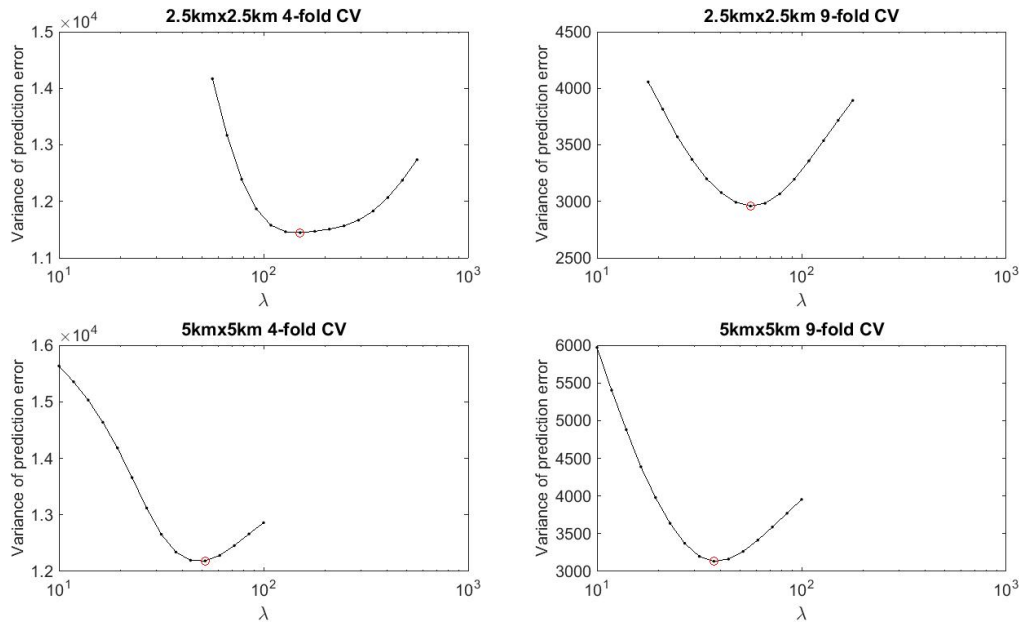
Figure 5.1.: Estimated optimum penalties for each combination of spatial resolution at the reservoir level and for each cross-validation scheme. The optimum penalties λ_{optim} are indicated by a red circle on each graph.

The fit of the models using the optimal penalty to the optical leveling measurements for various combinations of epochs are given in figures 5.2 and 5.3 for the 2.5km reservoir and 4-fold cross-validation scheme. The fit to the data for the other reservoir resolution and CV-schemes are given in figures C.1 through to C.6. Overall, the fit is very similar between the various model-resolutions and CV-schemes, with no obvious outliers in the residuals and some spatial structure in the residuals which appears to be restricted to spatial scales well below the resolution of the 9-fold CV-scheme.

A comparison of estimated compaction per aggregated reservoir section for the 1972-09-01 - 2008-08-13 epoch for both reservoir resolutions and cross-validation schemes is given in figure 5.4. The estimates for the 9-fold CV schemes are more variable than those of the 4-fold CV-schemes because of the lower estimated optimum penalties for the 9-fold CV-schemes. Overall, the 4-fold CV-schemes have therefore resulted in the most spatially smooth set of parameter estimates. Although the differences between the four models are relatively small, the results for the 2.5km reservoir resolution and 4-fold CV-scheme have the largest RMSE for the inversion fit (RMSE1 in table 5.2) indicating that this combination of reservoir resolution and CV-scheme resulted in the spatially smoothest representation of the subsidence bowl. This is illustrated in a number of prediction profiles of the subsidence bowl which have been generated for a number of cross-sections through the landscape (figures 5.5, 5.6 and 5.7). Predicted subsidence profiles for the different models are similar, but the 2.5km reservoir resolution and 4-fold CV-scheme resulted in the smoothest prediction profiles which can be best seen in the illustrated cross-section which runs from the south-west to the north-east of the subsidence bowl (figures 5.5c, 5.6c and 5.7c). Because the 2.5km reservoir resolution and 4-fold CV-scheme resulted in spatially smoothest set of estimates while allowing for a more precise geographical location of the deepest part of the subsidence bowl compared to the 5km resolution, we have chosen to discuss the results of the 2.5km resolution 4-fold CV-scheme in the main text as our preferred estimates. A map of compaction es-

Table 5.2.: An overview of estimated optimum penalties λ_{optim}, the number of aggregated reservoir sections n_a and root-mean-square errors (RMSE) of the fitted model, for each combination of reservoir resolution and cross-validation (CV) scheme. RMSE1: RMSE of the compaction model using the optimal penalty RMSE $= \sqrt{S}$ where $S_{\lambda_{optim}} = \left\| \mathbf{X^a \hat{L}^a_{\lambda_{optim}}} - \mathbf{Y} \right\|^2$ for the 1972-09-01 - 2008-08-13 epoch. RMSE2: RMSE of the predictions of the first-order forward model based on constant rates of compaction per unit of pore pressure decline (equation 4.11) for the 1972-09-01 - 2008-08-13 epoch. RMSE2: RMSE of the predictions of the first-order forward model based on constant rates of compaction per unit of pore pressure decline for the 1972-09-01 - 2013-03-03 epoch.

Resolution	n_a	CV-scheme	λ_{optim}	RMSE1 (m)	RMSE2 (m)	RMSE3 (m)
2.5km	227	4-fold	151	0.012	0.017	0.014
2.5km	227	9-fold	56	0.009	0.015	0.012
5km	58	4-fold	52	0.010	0.015	0.012
5km	58	9-fold	37	0.010	0.015	0.012

timates for the various epoch combinations is given in figure 5.8 (2.5km 4-fold CV; maps for the other models are given in figures B.1,B.2 and B.3).

5.3. Forward model for compaction as a function of pore pressure decline

To first order, the assumption that rates of compaction are constant with pressure decline appears reasonable for most aggregated reservoir sections. The fit of the estimated rates $\hat{\beta}_q$ (equation 4.11) to the compaction estimates is visualised in figures D.2 through to D.8 for all aggregated reservoir sections. An overview of the relationship between estimated compaction $\mathbf{\hat{L}^a}$ and depletion for all epochs (table 5.1) is given in figure 5.9. Maps of estimated rates $\hat{\beta}_q$ for the 2.5km reservoir resolution and 4-fold CV-scheme and 9-fold CV-scheme are given in figure 5.10. A comparison of estimated rates $\hat{\beta}_q$ for the four different combinations of reservoir resolution and cross-validation scheme is given in figure 5.11.

Estimates of compaction in sections on or near the edge of the grid can be expected to have higher variance than estimates in the other reservoir sections because the regularising effect due to the spatial smoothing is less in these reservoir sections (see section 4.3). In addition, sections near the edges of the grid, in particular the western side of the Groningen reservoir have experienced less pore pressure decline than other parts of the reservoir, and the relative uncertainty in estimated pressure decline in these sections is likely to be high. At the time of writing this report, adequate statistical methodology for estimation of the uncertainty surrounding estimates of reservoir compaction has not yet been implemented. Differences between the estimates of rates of compaction per unit pressure decline obtained under the two CV-schemes tend to be largest in aggregated reservoir sections on or near the edge of the reservoir grid (figure 5.10).

The first-order forward models based on constant rates of compaction per unit pore pressure decline per aggregated reservoir section are able to explain the variation in measured subsidence for the various epochs reasonably well (table 5.3 and Appendix E). There is little difference between the forward models based on the four different inversion methods in terms of how well they are able to explain the subsidence measurements (see also table 5.2). The first-order forward models perform at least as well if not better than the NAM models with prediction errors (RMSE) of 0.014 m (2.5km reservoir resolution and 4-fold CV-scheme) for the 1972-09-01 - 2013-03-03 epoch compared to 0.022 m - 0.023 m for the NAM models. The predictions of the first-order forward models are however somewhat biased with over- or under-estimation in various epochs
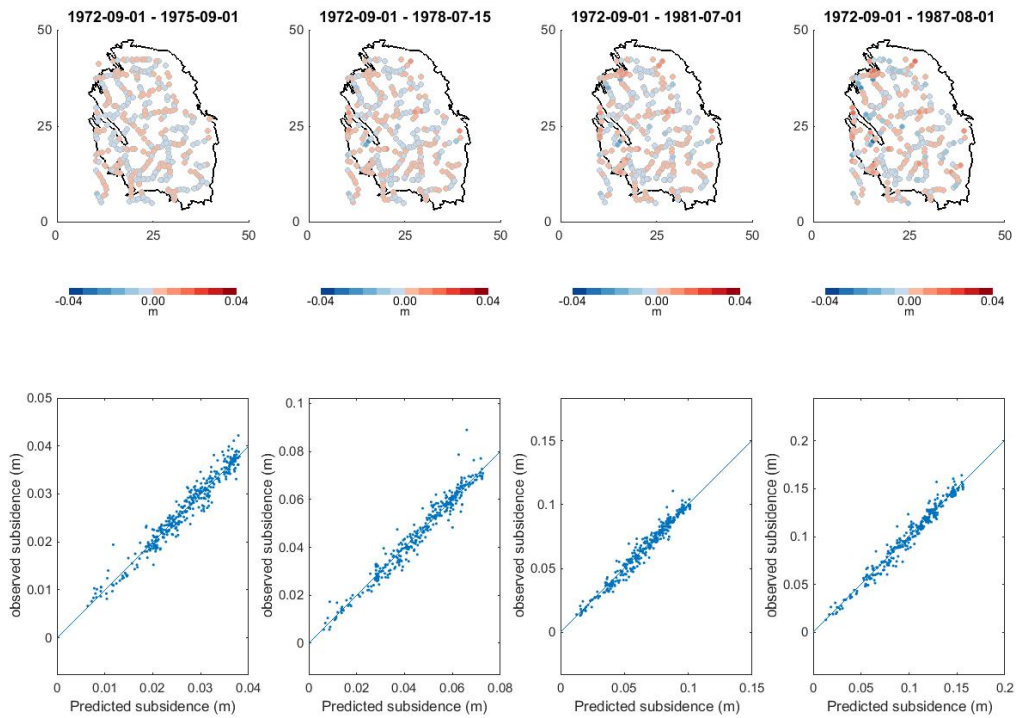
Figure 5.2.: Model fit and map of model residuals for the inversion to compaction using 9-fold spatial cross-validation for a 5km reservoir resolution for epochs up to 1987-08-01.

and a spatial pattern in the residuals albeit less pronounced than the current NAM models (figure E.1 through to figure E.8).
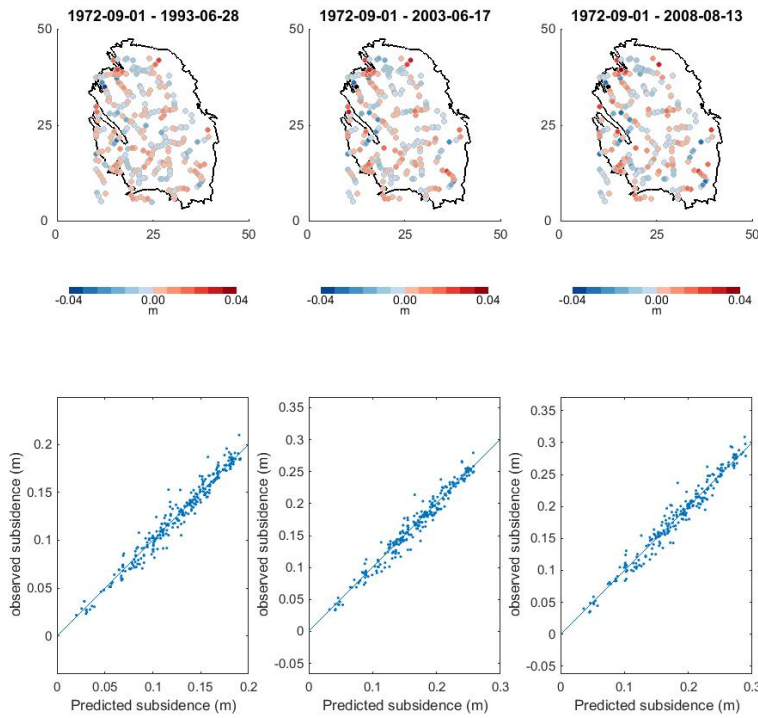
Figure 5.3.: Model fit and map of model residuals for the inversion to compaction using 9-fold spatial cross-validation for a 5km reservoir resolution for epochs up to 2008-08-13.
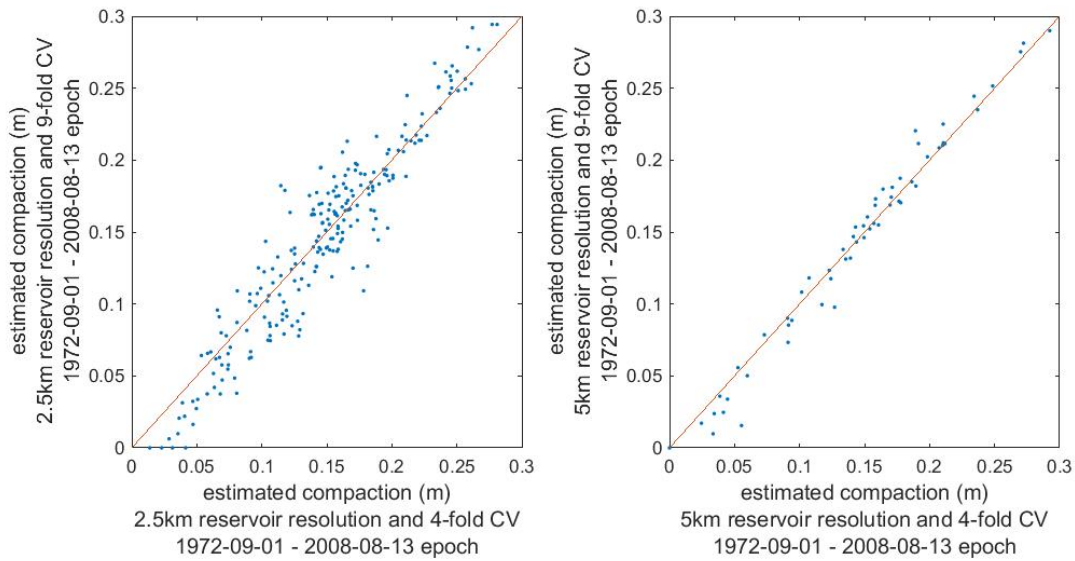
Figure 5.4.: Comparison of estimated compaction $\hat{\mathbf{L}}^{\mathbf{a}}$ at aggregated reservoir sections for both reservoir resolutions and cross-validation schemes, for the 1972-09-01 - 2008-08-13 epoch.
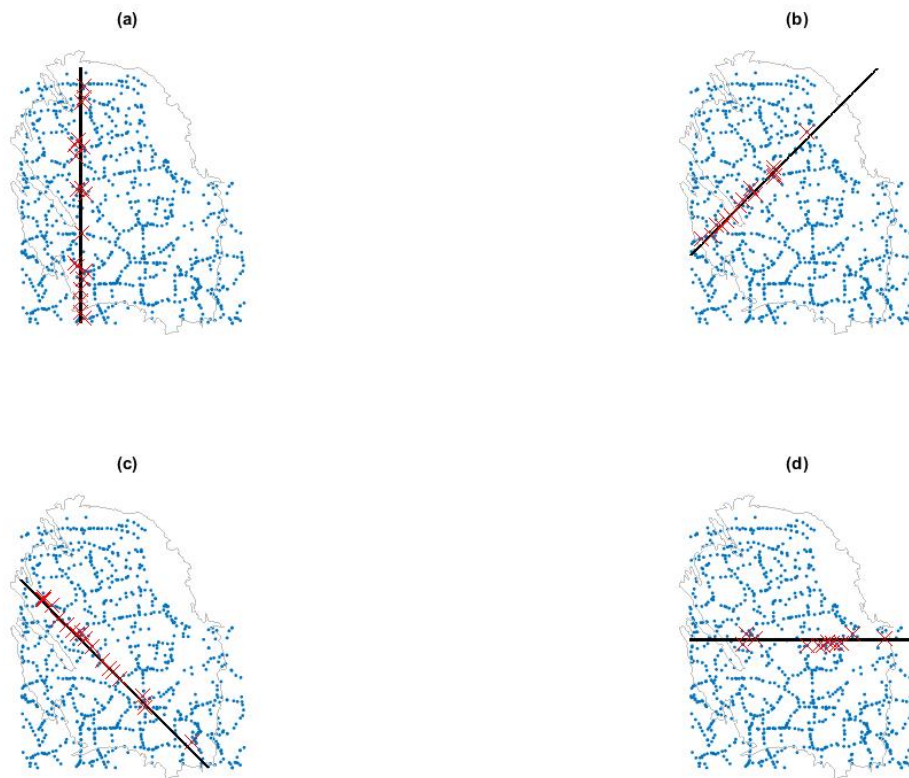
Figure 5.5.: Maps of cross-sections for which prediction profiles of the subsidence bowl have been generated for the 1972-09-01 - 2008-08-13 epoch (figures 5.6 and 5.7).

Table 5.3.: Root-mean-square-error (RMSE) of the current NAM forward models and the first-order forward models with constant rates of compaction per unit pore pressure decline per aggregated reservoir section (2.5km and 5km resolution and 4-fold CV-scheme).

epoch start	epoch end	TimeDecay RMSE (m)	Bilinear RMSE (m)	Isotach RMSE (m)	Inversion (2.5km) RMSE (m)	Inversion (5km) RMSE (m)
1972-09-01	1975-09-01	0.004	0.004	0.004	0.005	0.005
1972-09-01	1978-07-15	0.009	0.009	0.007	0.006	0.006
1972-09-01	1981-07-01	0.011	0.011	0.010	0.008	0.008
1972-09-01	1985-09-01	0.012	0.014	0.014	0.009	0.008
1972-09-01	1987-08-01	0.013	0.014	0.015	0.009	0.009
1972-09-01	1990-05-15	0.015	0.015	0.016	0.010	0.009
1972-09-01	1991-05-14	0.016	0.016	0.017	0.010	0.009
1972-09-01	1993-06-28	0.016	0.015	0.017	0.010	0.009
1972-09-01	1997-06-13	0.018	0.020	0.019	0.013	0.012
1972-09-01	1998-06-05	0.021	0.019	0.021	0.012	0.011
1972-09-01	2003-06-17	0.023	0.022	0.023	0.014	0.013
1972-09-01	2008-08-13	0.027	0.024	0.026	0.017	0.015
1972-09-01	2013-03-03	0.023	0.022	0.022	0.014	0.012
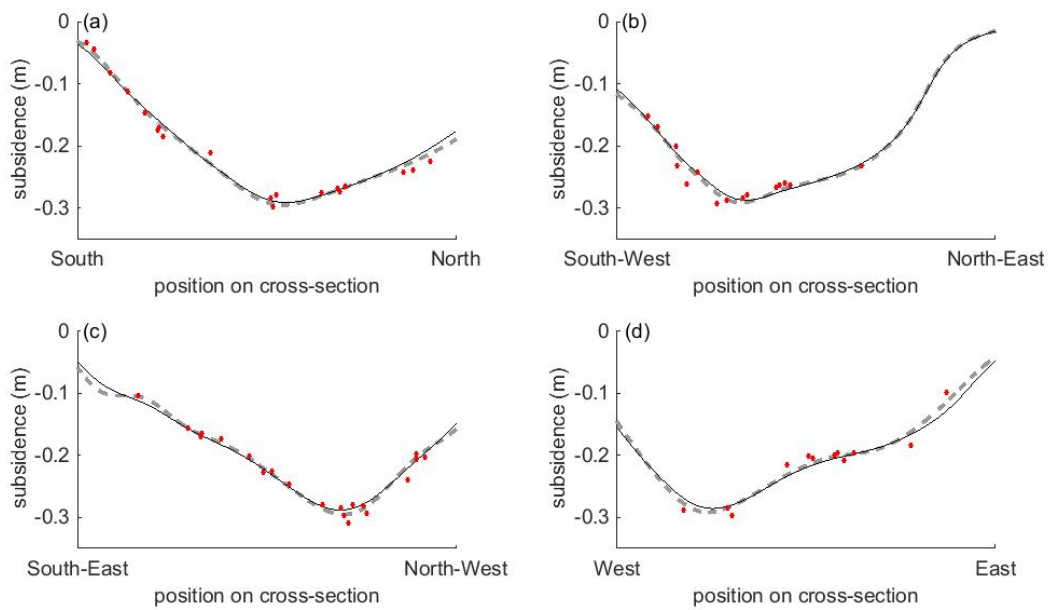
Figure 5.6.: Predicted profiles along cross-sections of the subsidence bowl for the 1972-09-01 - 2008-08-13 epoch. The cross-sections are indicated in figure 5.5. Predictions were made using the models with a 2.5km reservoir resolution and 4-fold CV (black lines) and 9-fold CV (grey dashed lines). Measurements of subsidence (red dots) are from benchmarks whose distance perpendicular to the cross-section (in the horizontal plane) was less than 1000 meters.
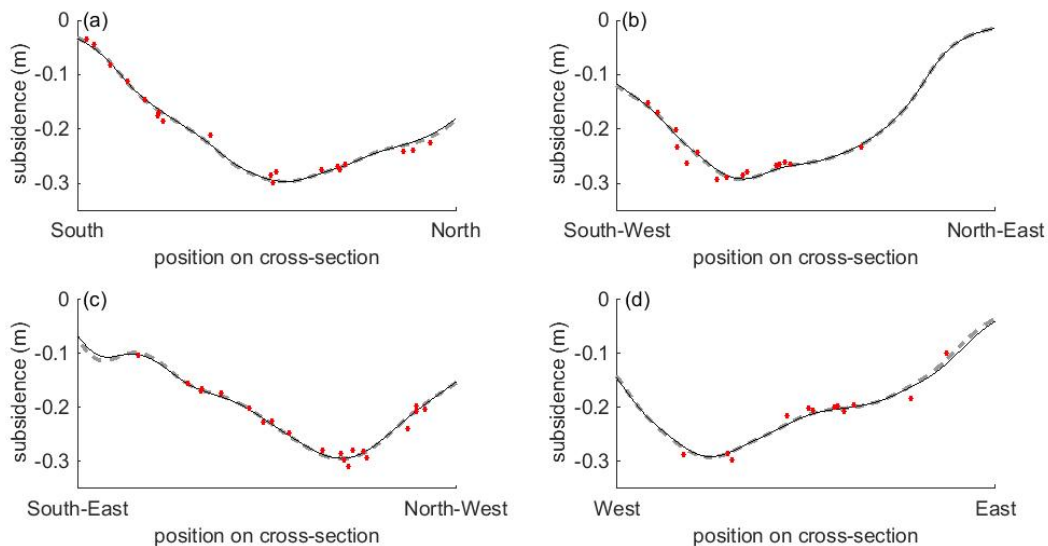
Figure 5.7.: Predicted profiles of the subsidence bowl along cross-sections for the 1972-09-01 - 2008-08-13 epoch. The cross-sections are indicated in figure 5.5. Predictions were made using the models with a 5km reservoir resolution and 4-fold CV (black lines) and 9-fold CV (grey dashed lines). Measurements of subsidence (red dots) are from benchmarks whose distance perpendicular to the cross-section (in the horizontal plane) was less than 1000 meters.
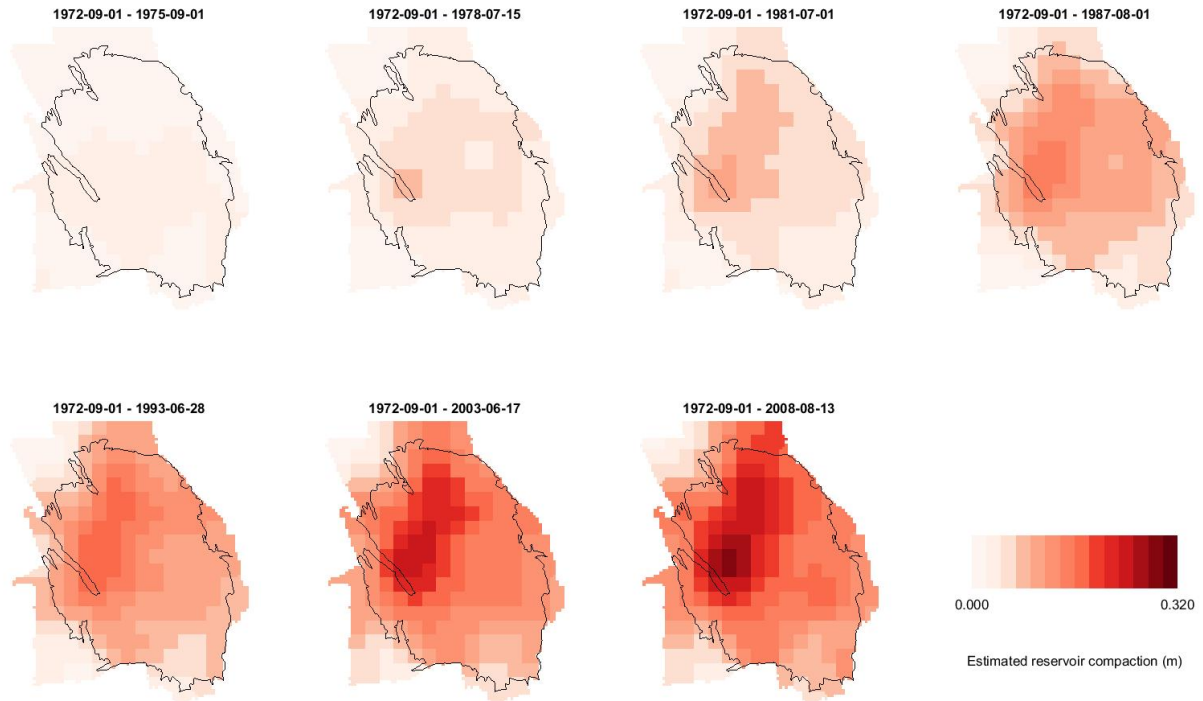
Figure 5.8.: Estimated compaction for 4-fold spatial cross-validation and a 2.5km reservoir resolution.
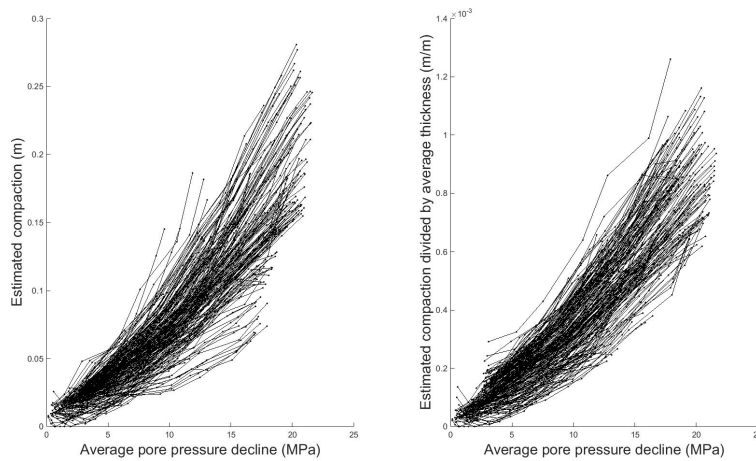
Figure 5.9.: Estimated compaction $\hat{\mathbf{L}}^{\mathbf{a}}$ per unit pore pressure decline for all epochs (table 5.1) and all aggregated reservoir sections (estimates of $\hat{\mathbf{L}}^{\mathbf{a}}$ per reservoir section for epochs with consecutive end dates are connected by lines) for the inversion to compaction using 4-fold spatial cross-validation and a 2.5km reservoir resolution.
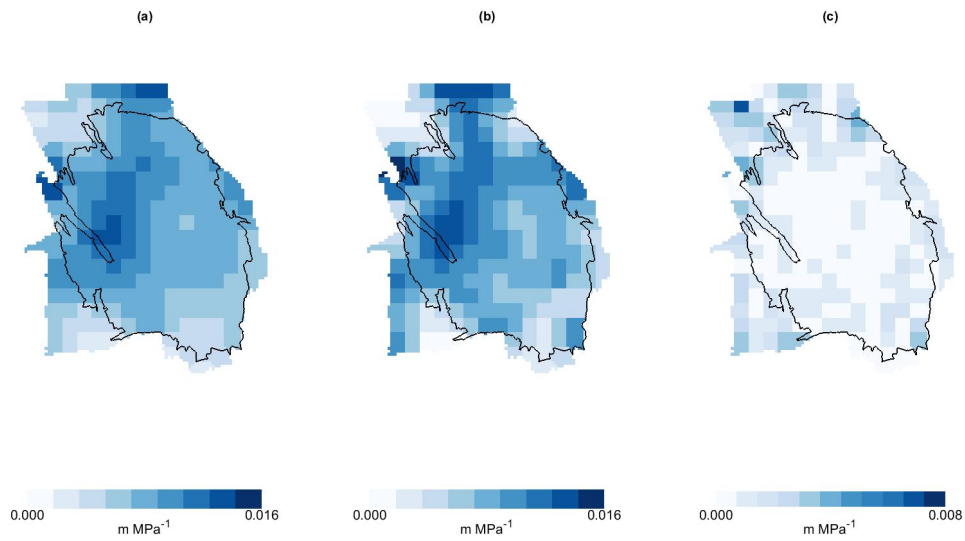
Figure 5.10.: Estimated rates of compaction per unit pore pressure decline $\hat{\beta}_q$ for the inversion to compaction for a 2.5km reservoir resolution and 4-fold (a) and 9-fold (b) CV-scheme, and the absolute differences in estimates obtained using both CV-schemes (c).
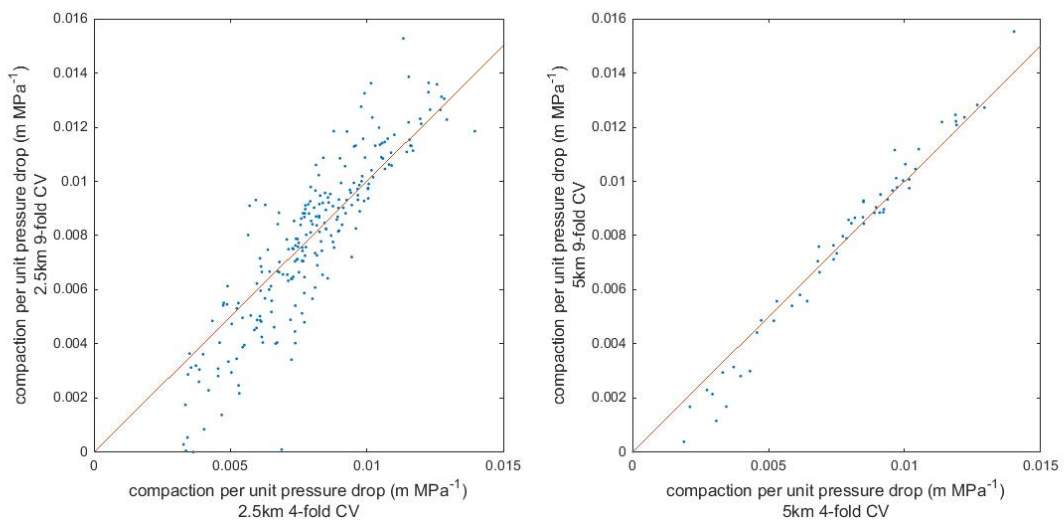
Figure 5.11.: Comparison of estimated rates of compaction per unit pore pressure decline per aggregated reservoir section ($\hat{\beta}_q$: equation 4.11).

6. Discussion

Statistical methodology is presented that may be used to estimate reservoir compaction through direct inversion using subsidence measurements from optical leveling campaigns. The main motivation for choosing this methodology was that models currently in use by NAM produce biased estimates of the subsidence bowl as evidenced by the existence of spatio-temporal patterns in the residuals of these models, indicating that these models are likely misspecified and/or that model input such as rock porosity maps or pressure grids are biased. Direct inversion to compaction provides a useful alternative view on the available information because estimates of compaction can be obtained without reliance on certain assumptions that are made in the current models, in particular:

- There is no need to assume a functional form for the relationship between reservoir compactibility and rock porosity.
- There is no need to assume that the rock porosity per reservoir section is known.
- There is no need to assume a functional form for the relationship between reservoir compaction and pore pressure decline.

The main disadvantage and technical challenge of the proposed methodology is that the independent contribution of compaction in different reservoir sections to the observed subsidence bowl cannot be estimated with sufficient precision without imposing regularisation in the inversion methodology. Here, we have attempted to find spatially smooth solutions which were able to explain the overall progression of the shape of the subsidence bowl, as apparent through measurements from optical leveling campaigns, well. Regularisation will inevitably result in biased estimates of parameters, and estimates will vary with the choice of cross-validation scheme and penalty matrix. The choice of epochs used for the inversion is important too. If little subsidence has taken place during an epoch, the signal (progression of the subsidence bowl) will be weak in comparison to the noise (due to errors in measurements or subsidence caused by processes other than reservoir compaction). In practice, more spatial smoothness will be imposed in cases where the signal to noise ratio is weak, and this means that the amount of bias of estimates due to spatial smoothing will tend to be higher if the realised pressure decline during an epoch gets smaller. The effect of this needs to be better investigated by applying the regularisation to different combinations of epochs and by allowing the penalty λ_{optim} to vary between epochs.

The regularisation methodology was effective in enabling the estimation of spatially resolved compaction estimates without over-fitting of the optical leveling measurements: spatially smooth estimates of compaction and the subsidence bowl were obtained for both reservoir resolutions and CV-schemes. The spatio-temporal progression of the subsidence bowl could be described well by a spatio-temporally smooth set of compaction estimates. The 4-fold CV-scheme resulted in the smoothest set of compaction estimates. This was as expected because the smaller quadrants used in the 9-fold CV-scheme allowed for more local curvature, as apparent in the subsidence measurements, to be picked up. The spatially smoothest set of compaction estimates was obtained at the 2.5km reservoir resolution in combination with a 4-fold CV-scheme and we present these results in the main text as our preferred estimates. For all reservoir resolutions and CV-schemes, estimates of compaction correlated strongly with pore pressure decline. A first-order forward simulation model was defined with constant rates of compaction per unit of pore pressure decline per

reservoir section. This first-order forward model performed well in comparison with the current models in use by NAM in its ability to explain the variation in subsidence measurements.

Our results indicate that direct inversion to compaction provides a useful alternative methodology to estimate reservoir compaction because certain key assumptions that are made in the current models in use by NAM can be relaxed. At a second modeling stage, the apparent existence (or absence) of relationships, and the functional form thereof, between reservoir compaction and variables such as reservoir pressures, thickness or porosity can be investigated. In this report, the investigation of such relationships has been restricted to a basic (first-order) model assuming constant rates of compaction per unit pore pressure decline per reservoir section, but a wider variety of models needs to be investigated.

The impact of the choice of influence matrix on the compaction estimates needs to be investigated.

We have identified the following topics for future work:

1. Direct inversion to compaction based on InSAR data. The variation of compaction estimates based on InSAR data and optical leveling data will indicate how robust these estimates are with respect to assumptions regarding measurement noise or the spatial and temporal coverage of surveys. InSAR data provide information on horizontal displacements which may be used to constrain the choice of influence matrix, especially at the edges of the subsidence bowl.

2. Develop methodology to estimate the uncertainty surrounding the compaction estimates obtained through regularised direct inversion.

3. Further investigate the relationship between compaction and depletion estimates, including non-linear relationships.

4. The results as presented in this report indicate that a forward model based on constant rates of compaction per unit pressure decline per aggregated reservoir section is able to describe the variation in the optical leveling measurements well. An alternative model for direct inversion to compaction with fewer parameters to be estimated can be based on the assumption of constant rates of compaction per unit pressure decline. In such a model, spatial smoothness can be imposed on the rates. Such spatial smoothness is not imposed in the current forward model.

Appendix A.

Additional graphs of the fit of current NAM models to leveling data

This appendix contains a number of additional graphs which visualise the ability of current NAM models to explain the variation in subsidence as measured in various optical leveling campaign epochs (see chapter 3). All NAM models have epochs during which they either systematically under-predict or over-predict subsidence in either all or part of the subsidence bowl, for example for the 1964-04-15 - 1972-09-01 epoch (A.1), the 1972-09-01 - 1975-09-01 epoch (Figure A.2), the 1987-08-01 - 1993-06-08 epoch (Figure A.3) or the 2003-06-17 - 2008-08-13 epoch (Figure A.4).
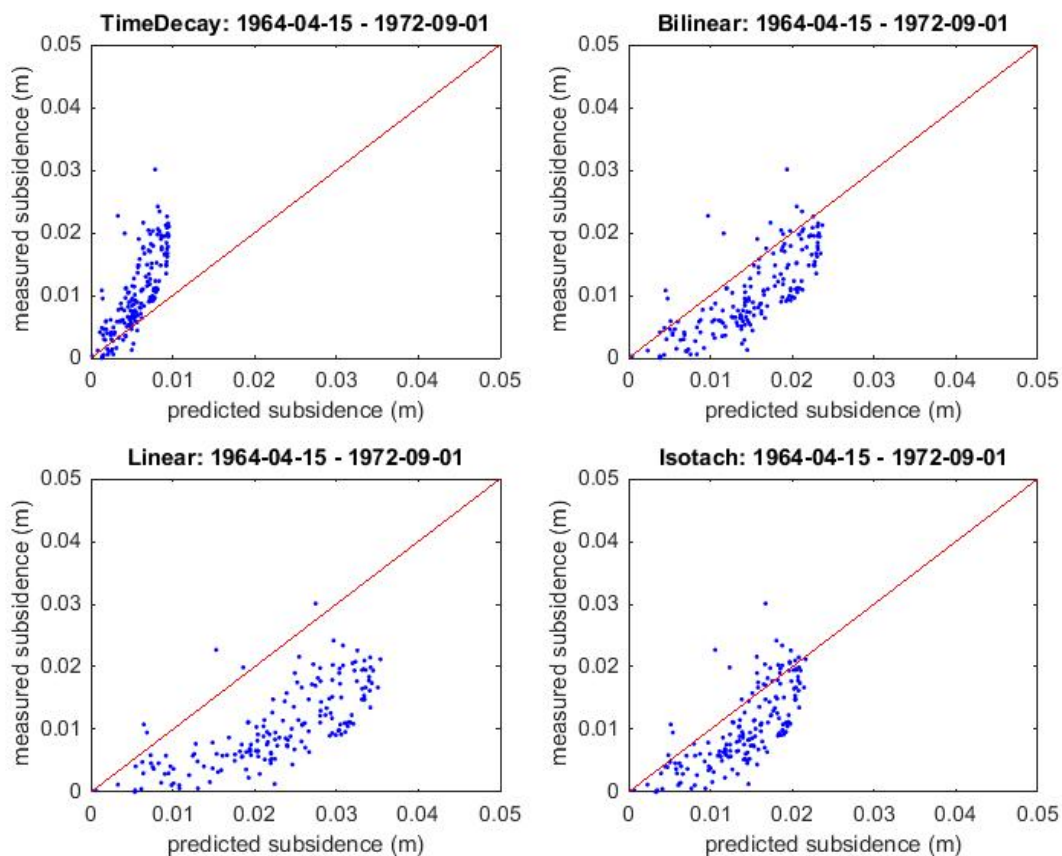
Figure A.1.: Predicted versus measured subsidence for all NAM models (1964-04-15 - 1972-09-01 epoch).
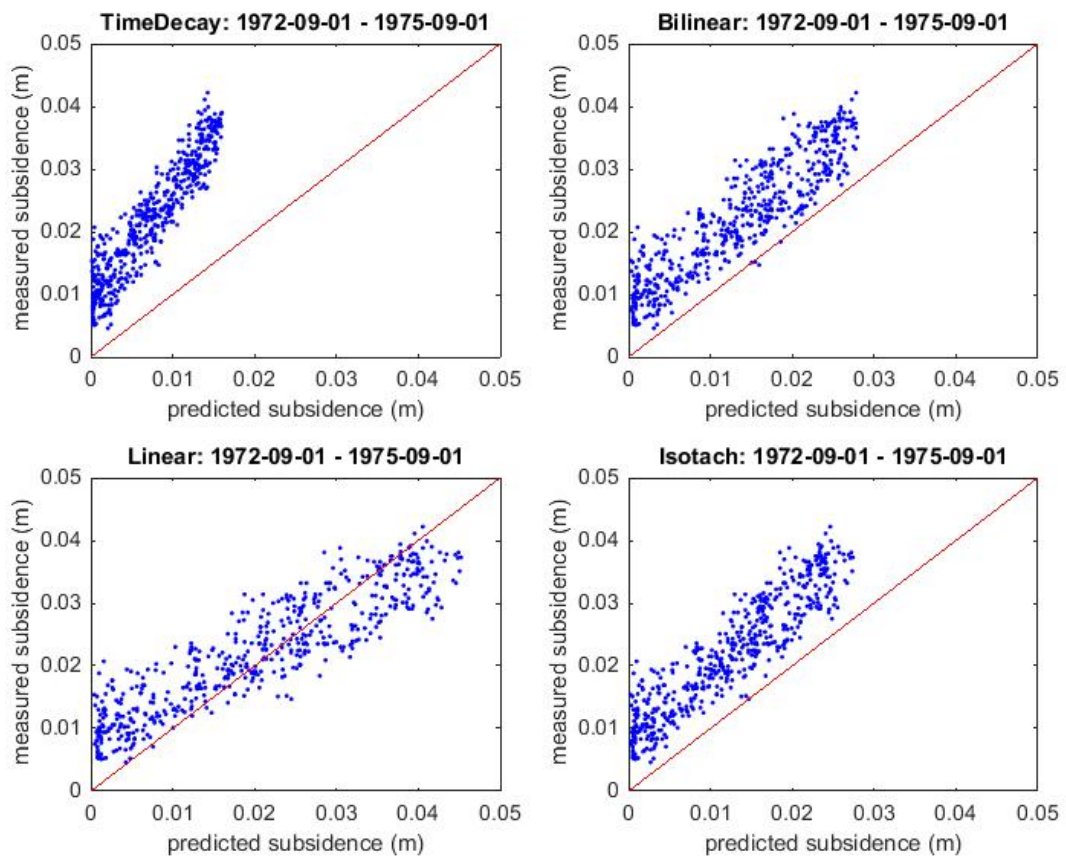
Figure A.2.: Predicted versus measured subsidence for all NAM models (1972-09-01 - 1975-09-01 epoch).
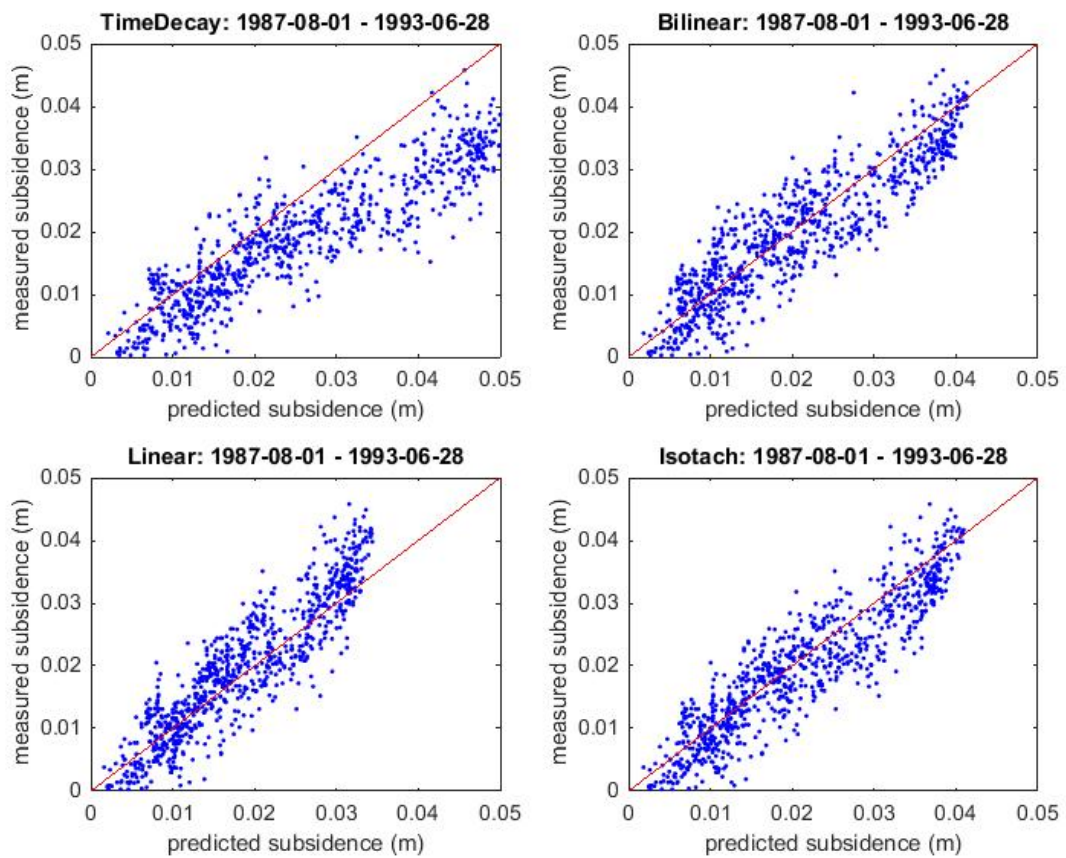
Figure A.3.: Predicted versus measured subsidence for all NAM models (1987-08-01 - 1993-06-08 epoch).
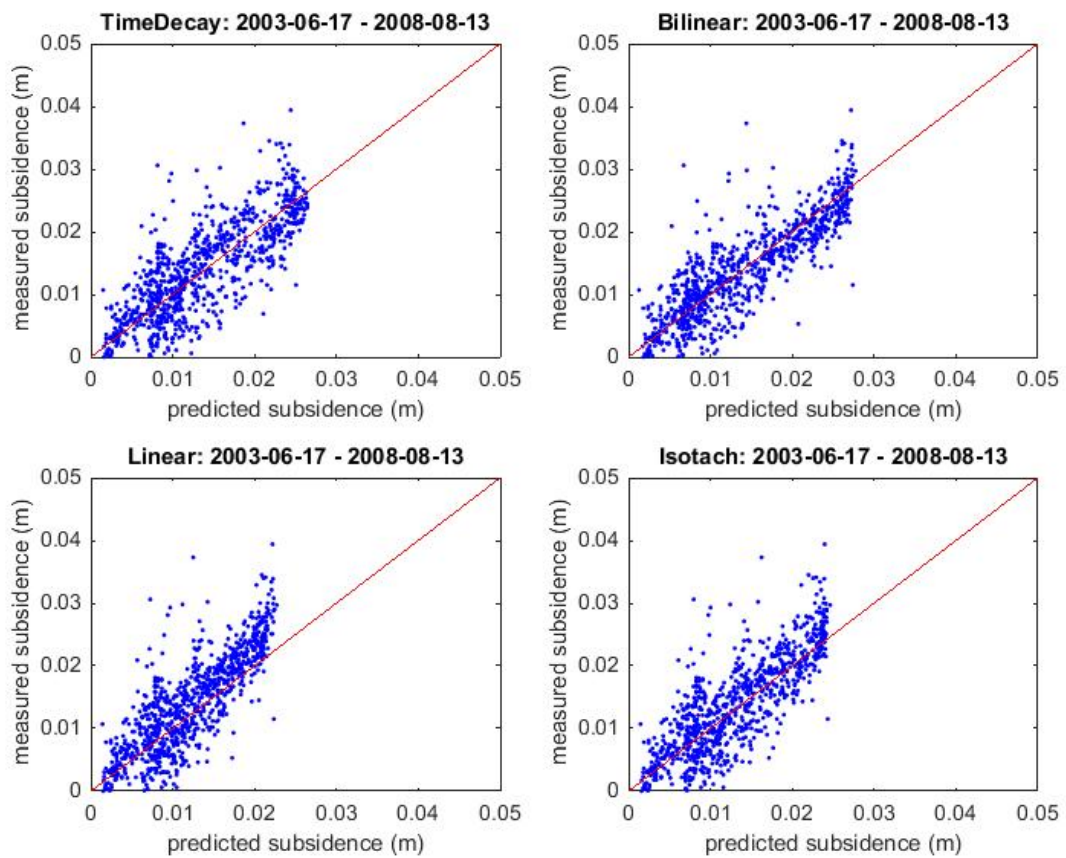
Figure A.4.: Predicted versus measured subsidence for all NAM models (2003-06-17 - 2008-08-13 epoch).

Appendix B.

Additional graphs on estimated compaction

This appendix contains maps which depict the estimates of compaction of aggregated reservoir section $\hat{\mathbf{L}}^{\mathbf{a}}$ for all combinations of reservoir resolutions and cross-validation schemes (table 5.2), except the 2.5km reservoir resolution with a 4-fold CV-scheme which is included in the main text (see chapter 5.2 and figure 5.8).
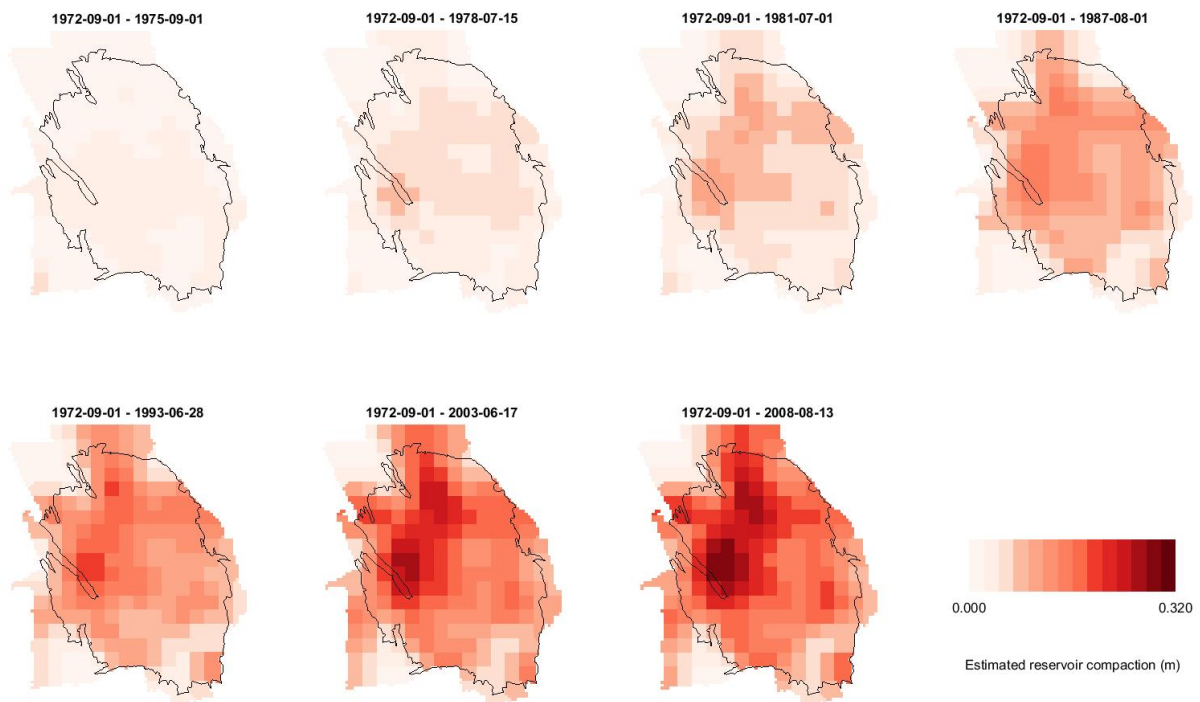
Figure B.1.: Estimated compaction for 9-fold spatial cross-validation and a 2.5km reservoir resolution.
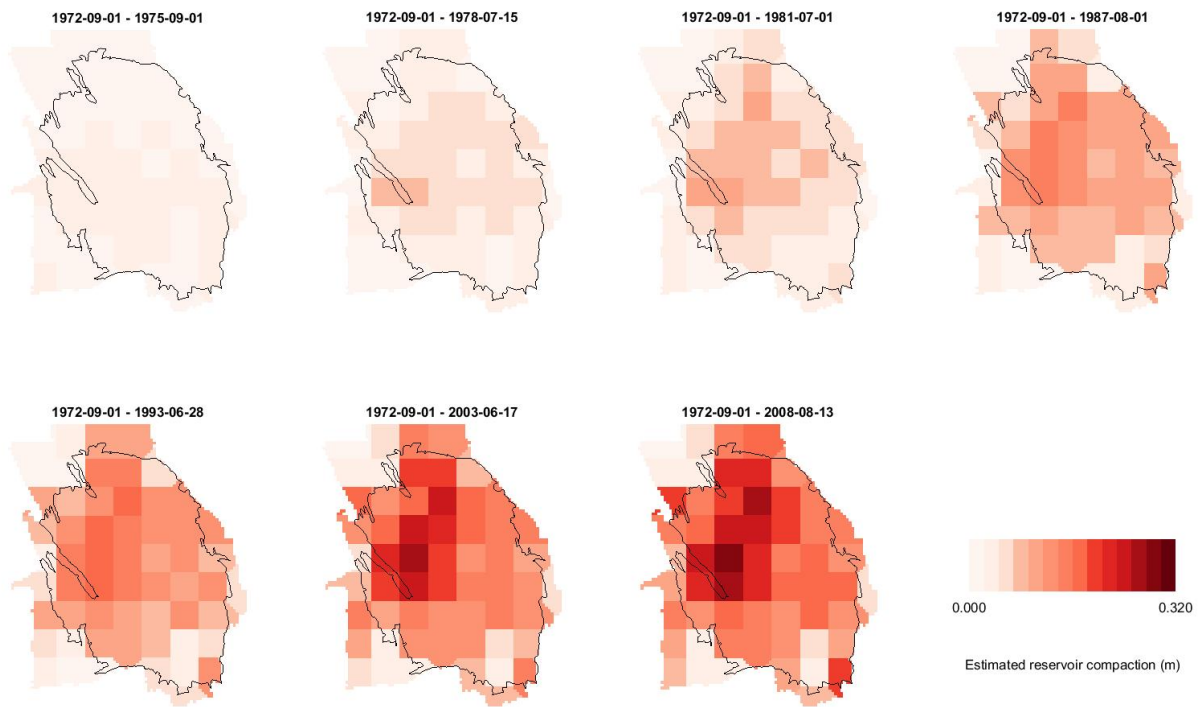
Figure B.2.: Estimated compaction for 4-fold spatial cross-validation and a 5km reservoir resolution.
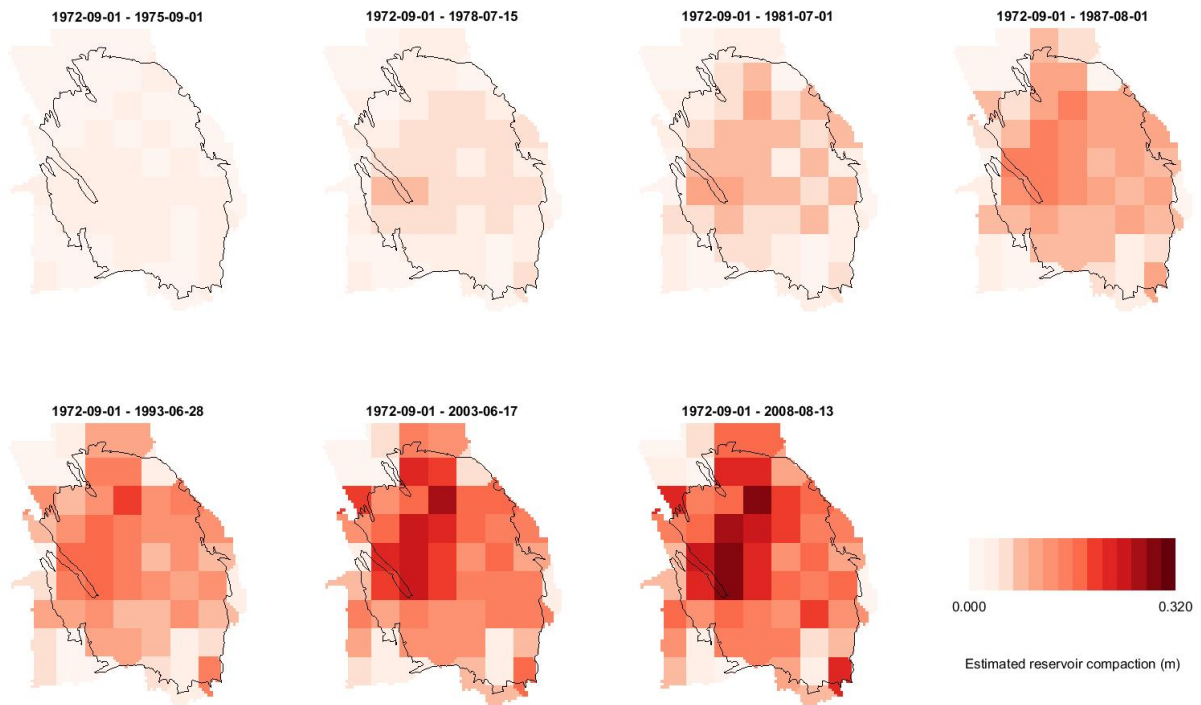
Figure B.3.: Estimated compaction for 9-fold spatial cross-validation and a 5km reservoir resolution.

Appendix C.

Additional graphs on residuals of inversion to compaction models

This appendix contains maps and graphs which depict the fit of the regularised inversion models to the optical leveling data for all combinations of reservoir resolutions and cross-validation schemes (table 5.2), except the 2.5km reservoir resolution with a 4-fold CV-scheme which is included in the main text (see chapter 5.2, figure 5.2 and figure 5.3).
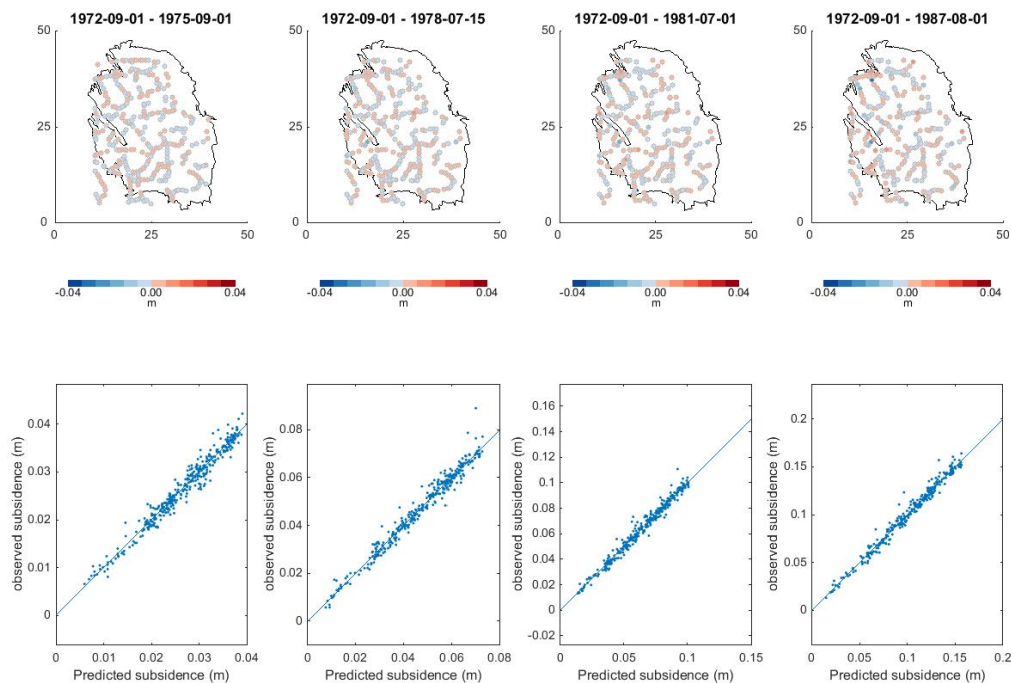
Figure C.1.: Model fit and map of model residuals for the inversion to compaction using 9-fold spatial cross-validation for a 2.5km reservoir resolution for epochs up to 1987-08-01.
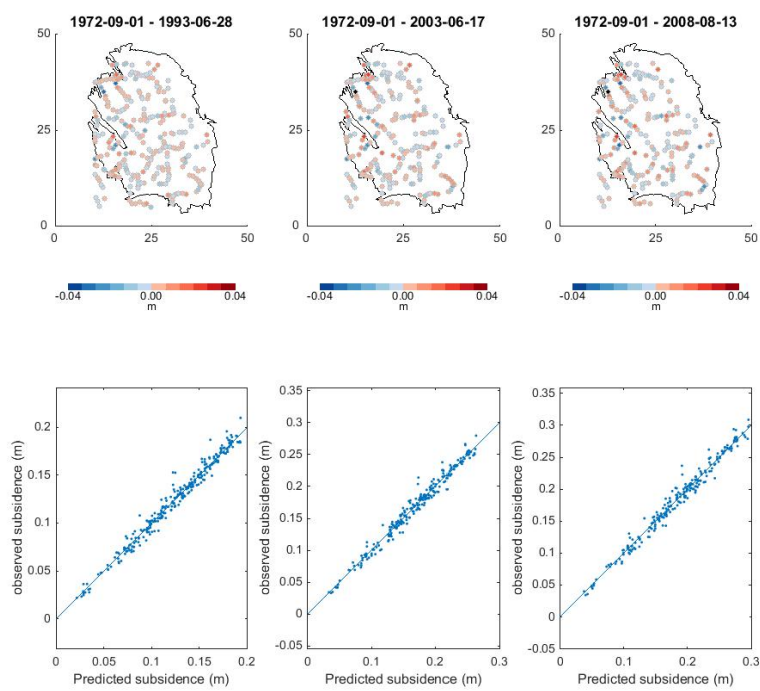
Figure C.2.: Model fit and map of model residuals for the inversion to compaction using 9-fold spatial cross-validation for a 2.5km reservoir resolution for epochs up to 2008-08-13.
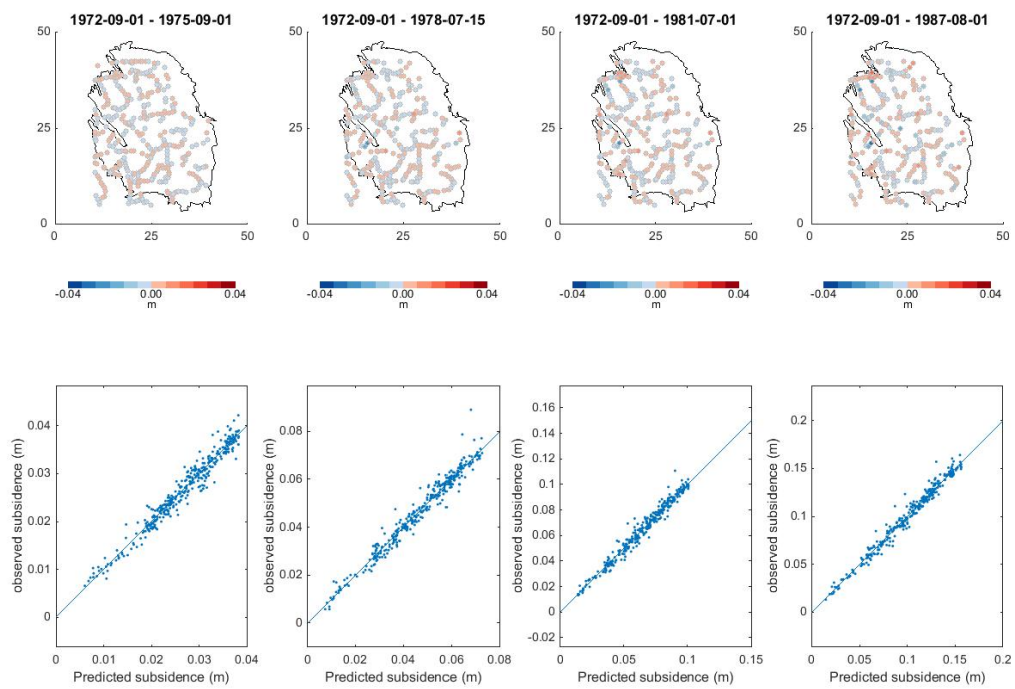
Figure C.3.: Model fit and map of model residuals for the inversion to compaction using 4-fold spatial cross-validation for a 5km reservoir resolution for epochs up to 1987-08-01.
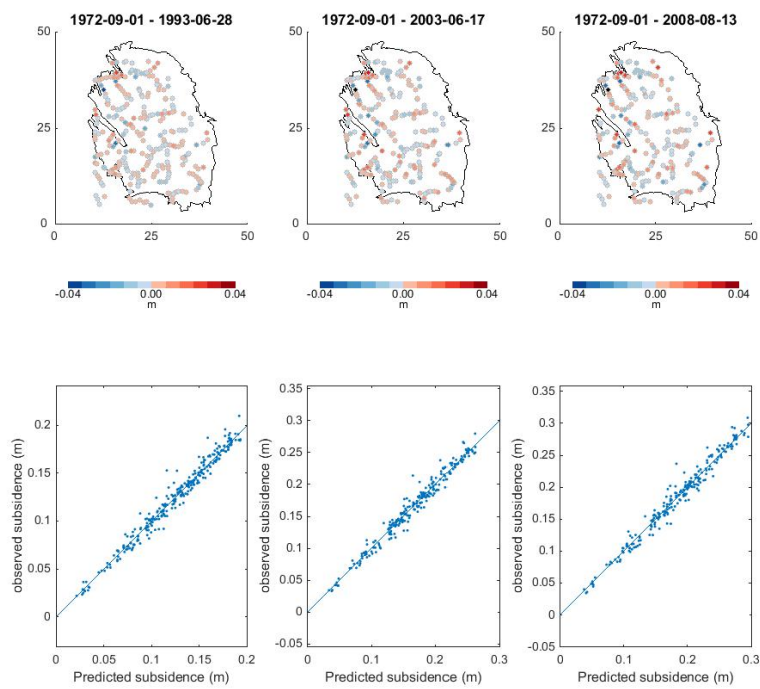
Figure C.4.: Model fit and map of model residuals for the inversion to compaction using 4-fold spatial cross-validation for a 5km reservoir resolution for epochs up to 2008-08-13.
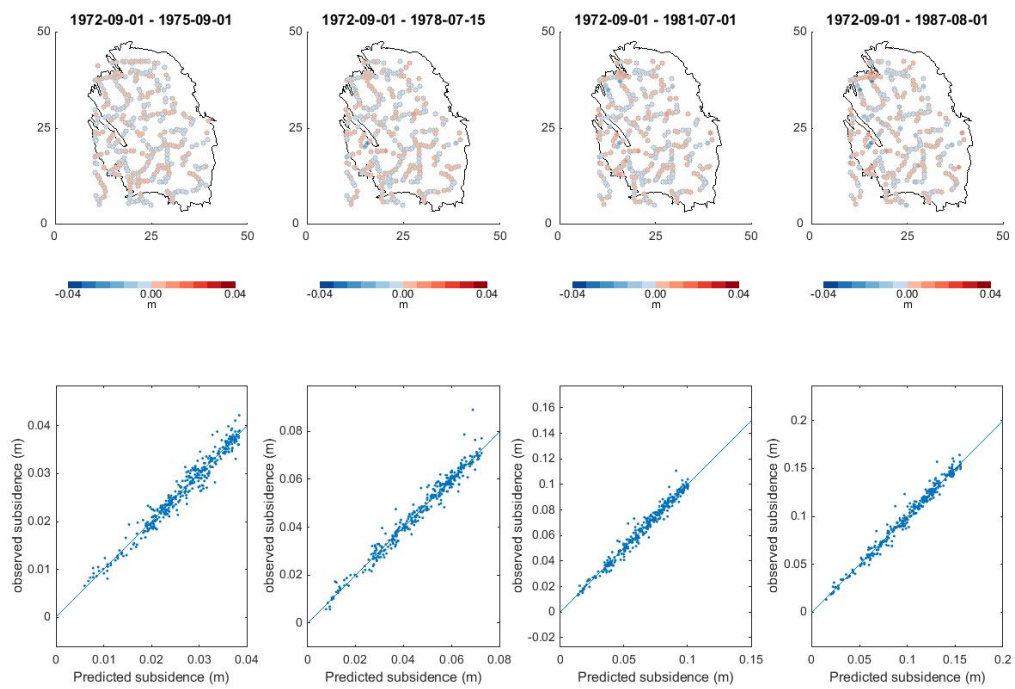
Figure C.5.: Model fit and map of model residuals for the inversion to compaction using 9-fold spatial cross-validation for a 5km reservoir resolution for epochs up to 1987-08-01.
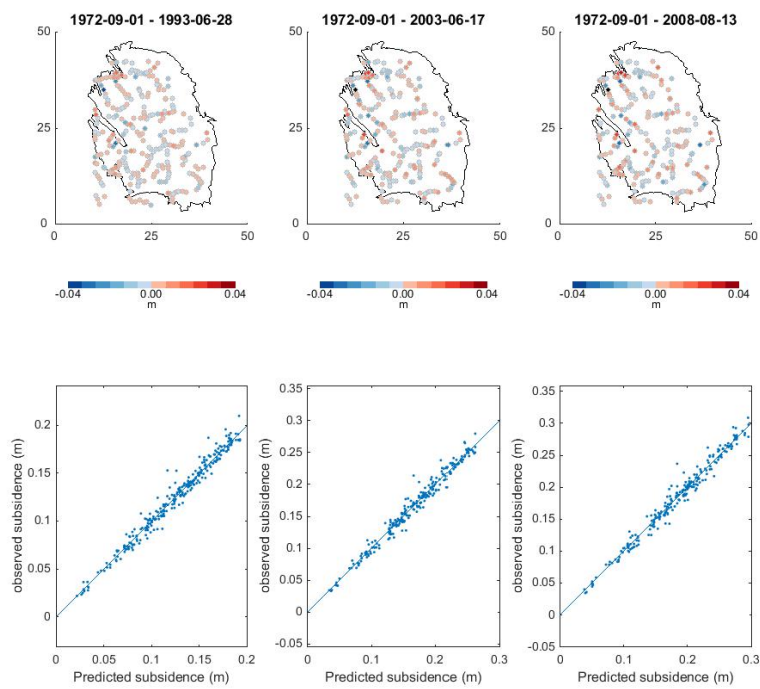
Figure C.6.: Model fit and map of model residuals for the inversion to compaction using 9-fold spatial cross-validation for a 5km reservoir resolution for epochs up to 2008-08-13.

Appendix D.

Additional graphs on estimated compaction per unit pore pressure decline

This appendix contains additional graphs which depict the relationship between estimated compaction $\hat{L}^a$ and pore pressure decline per aggregated reservoir section for the 2.5km 4-fold CV-scheme as discussed in section 5.3. To first order, the assumption that rates of compaction are constant with pressure decline appears reasonable for most reservoir sections. The fit of the estimated values $\hat{\beta}_q$ to the compaction estimates is visualised in figures D.2 through to D.8 for all aggregated reservoir sections. A spatial map of the estimated rates $\hat{\beta}_q$ is given in figure **??**. A comparison of estimated rates ($\hat{\beta}_q$ for the four different combinations of reservoir resolution and cross-validation scheme is given in figure 5.11.
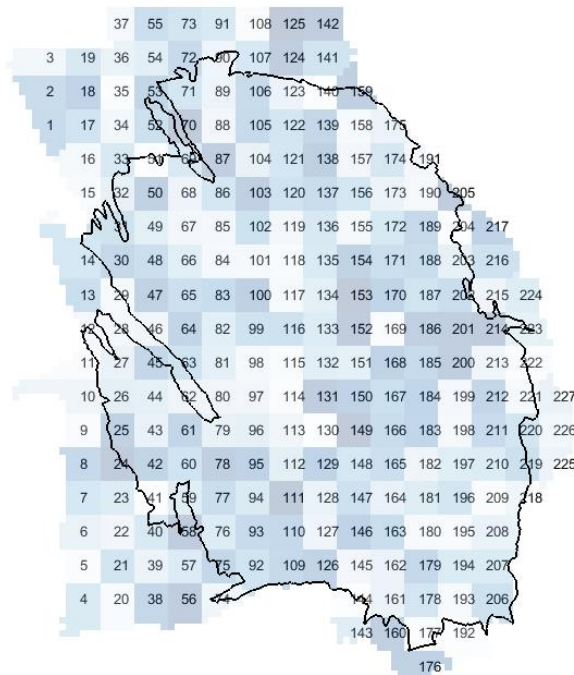
Figure D.1.: Labels q of aggregated reservoir sections, to be used for reference in figures D.2 through to D.8.
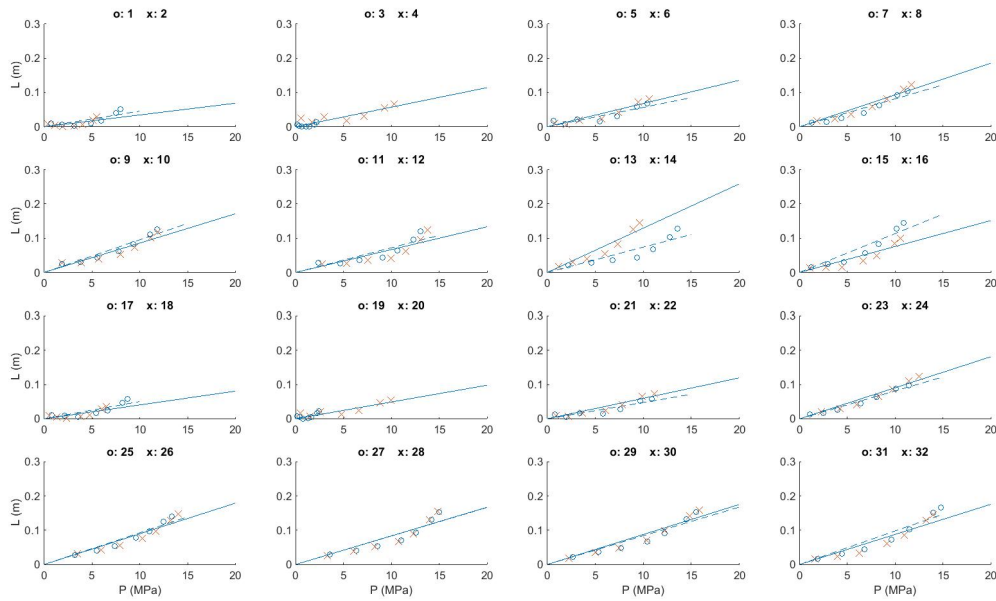
Figure D.2.: Relationship between the estimated compaction in reservoir section q, $\hat{\mathbf{L}}^{\mathbf{a}}$ and the pore pressure decline in that reservoir section $\mathbf{P}_q$ for aggregated reservoir sections $q = 1, 2, ..., 32$. The spatial location of reservoir section q can be found on the map in figure D.1.
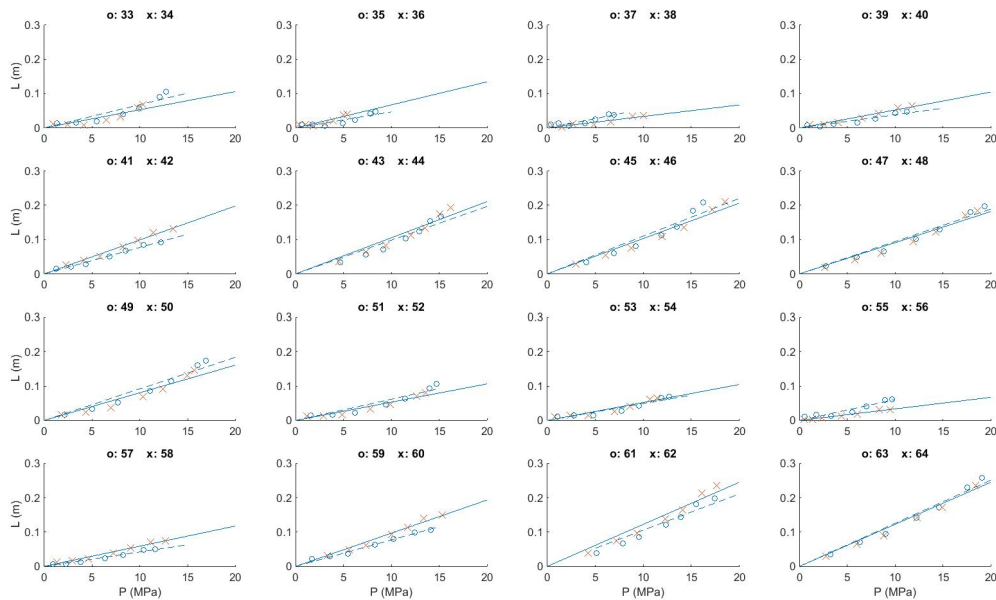
Figure D.3.: Relationship between the estimated compaction in reservoir section q, $\hat{\mathbf{L}}^{\mathbf{a}}$ and the pore pressure decline in that reservoir section $\mathbf{P}_q$ for aggregated reservoir sections $q = 33, 34, ..., 64$. The spatial location of reservoir section q can be found on the map in figure D.1.
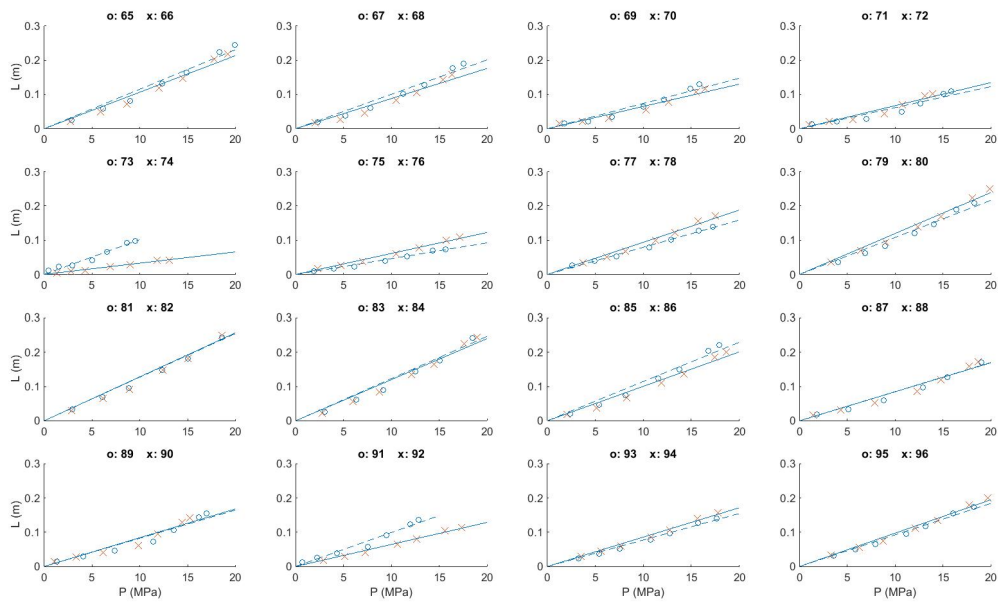
Figure D.4.: Relationship between the estimated compaction in reservoir section q, $\hat{\mathbf{L}}^{\mathbf{a}}$ and the pore pressure decline in that reservoir section $\mathbf{P}_q$ for aggregated reservoir sections $q = 65, 66, ..., 96$. The spatial location of reservoir section q can be found on the map in figure D.1.
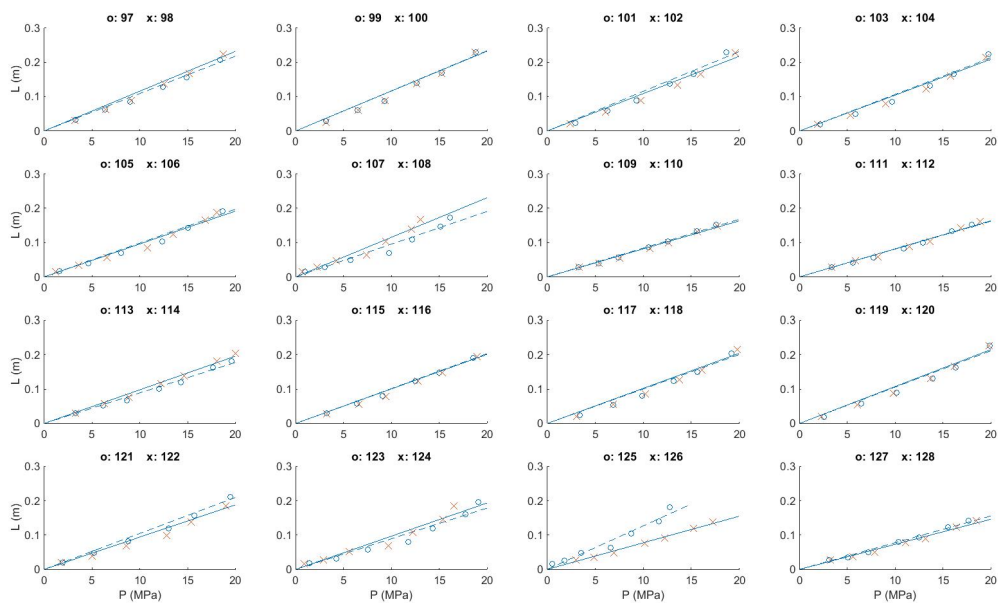
Figure D.5.: Relationship between the estimated compaction in reservoir section q, $\hat{\mathbf{L}}^{\mathbf{a}}$ and the pore pressure decline in that reservoir section $\mathbf{P}_q$ for aggregated reservoir sections $q = 97, 98, ..., 128$. The spatial location of reservoir section q can be found on the map in figure D.1.
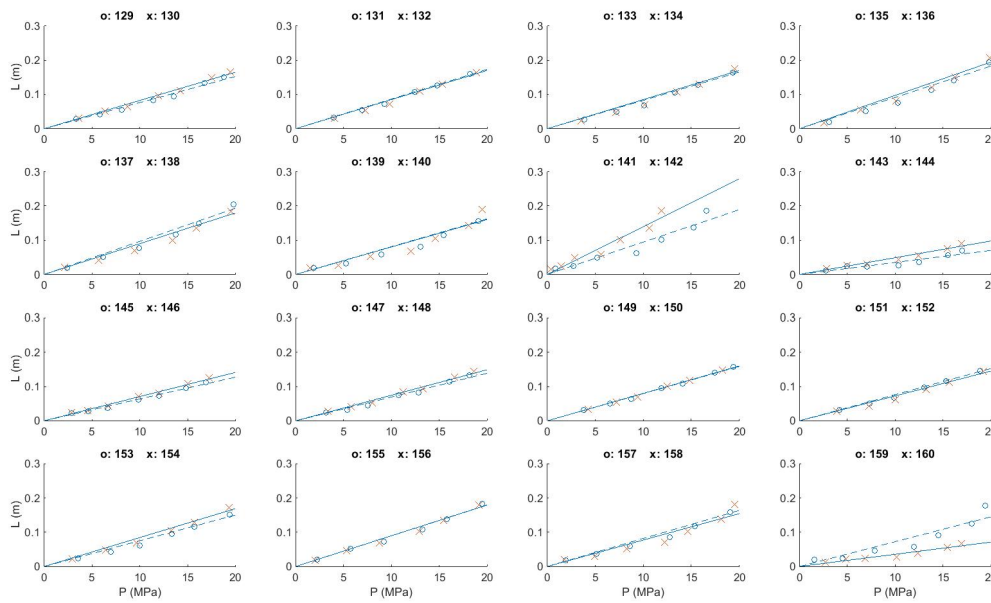
Figure D.6.: Relationship between the estimated compaction in reservoir section q, $\hat{\mathbf{L}}^{\mathbf{a}}$ and the pore pressure decline in that reservoir section $\mathbf{P}_q$ for aggregated reservoir sections $q = 129, 130, ..., 160$. The spatial location of reservoir section q can be found on the map in figure D.1.
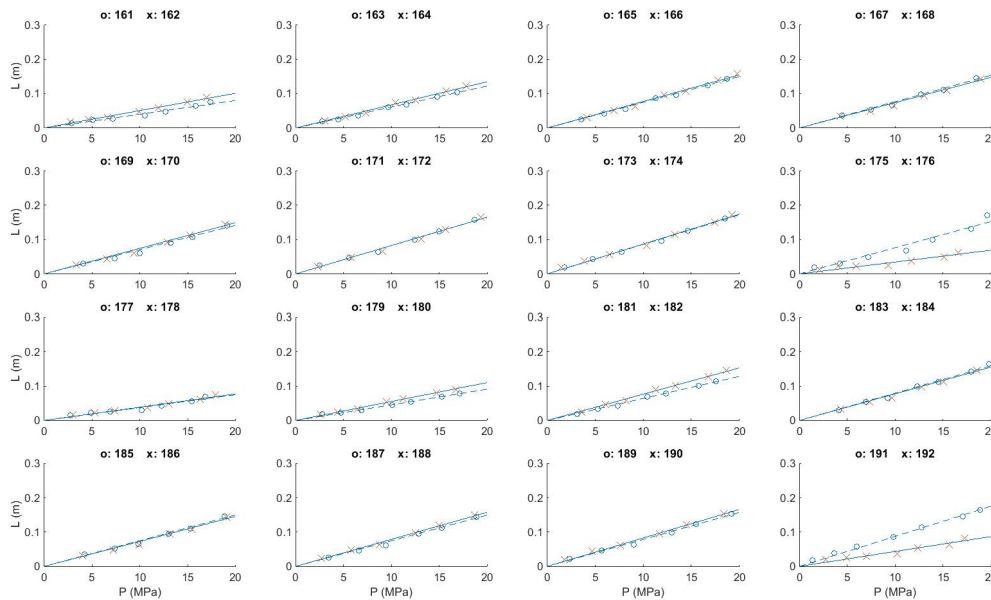
Figure D.7.: Relationship between the estimated compaction in reservoir section q, $\hat{\mathbf{L}}^{\mathbf{a}}$ and the pore pressure decline in that reservoir section $\mathbf{P}_q$ for aggregated reservoir sections $q = 161, 162, ..., 192$. The spatial location of reservoir section q can be found on the map in figure D.1.
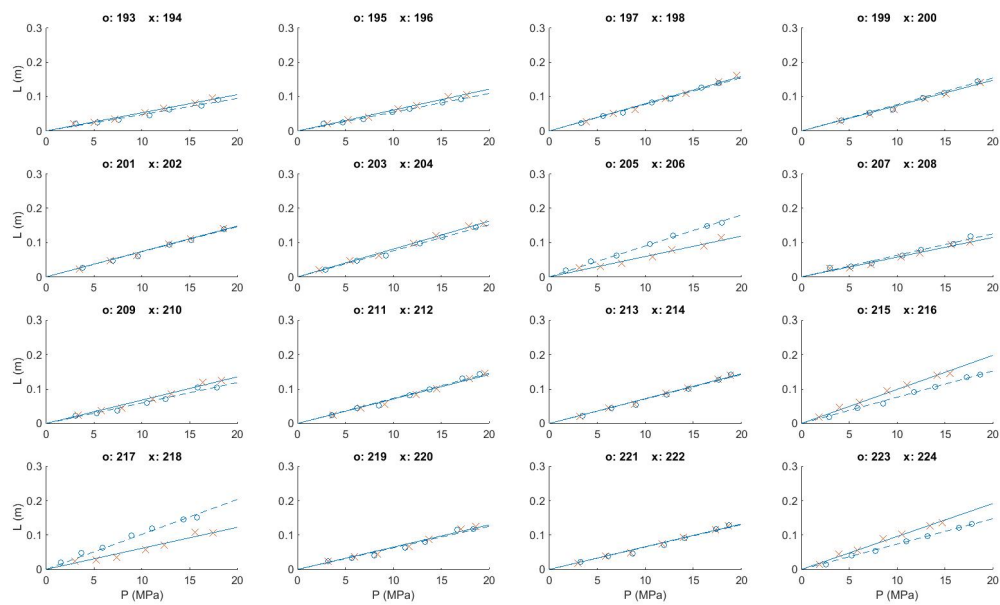
Figure D.8.: Relationship between the estimated compaction in reservoir section q, $\hat{\mathbf{L}}^{\mathbf{a}}$ and the pore pressure decline in that reservoir section $\mathbf{P}_q$ for aggregated reservoir sections $q = 193, 194, ..., 224$. The spatial location of reservoir section q can be found on the map in figure D.1.

Appendix E.

Additional graphs on the fit of the first-order forward prediction model

This appendix contains additional graphs which depict the fit of the first-order forward model based on constant rates of compaction per unit pore pressure decline per aggregated reservoir section $\hat{\beta}_q$ (figure E.1 through to figure E.8). Predicted subsidence is plotted against measurements from the optical leveling surveys for a number of epochs. The estimates of $\hat{\beta}_q$ are based on the model with a 2.5km reservoir resolution and 4-fold CV-scheme. The model fit for a number of the NAM models for each epoch is also given for reference.
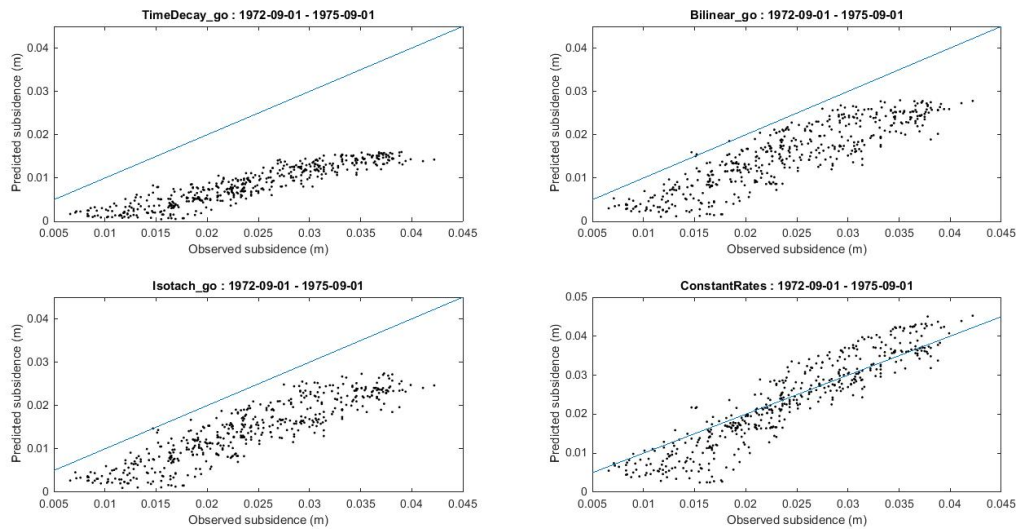
Figure E.1.: Predicted versus measured subsidence for NAM models and a model based on regularised direct inversion to compaction (ConstantRates: see text) for the 1972-09-01 - 1975-09-01 epoch.
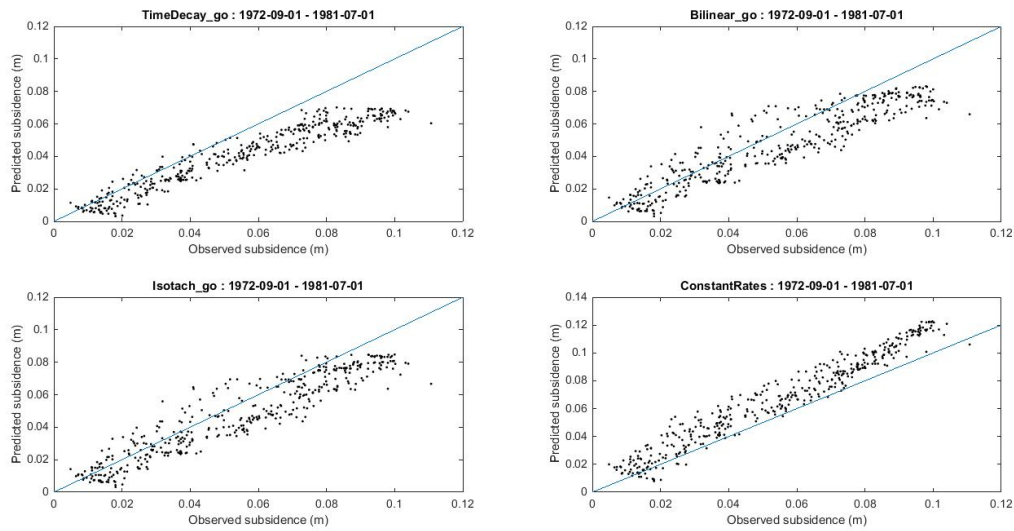
Figure E.2.: Predicted versus measured subsidence for NAM models and a model based on regularised direct inversion to compaction (ConstantRates: see text) for the 1972-09-01 - 1981-07-01 epoch.
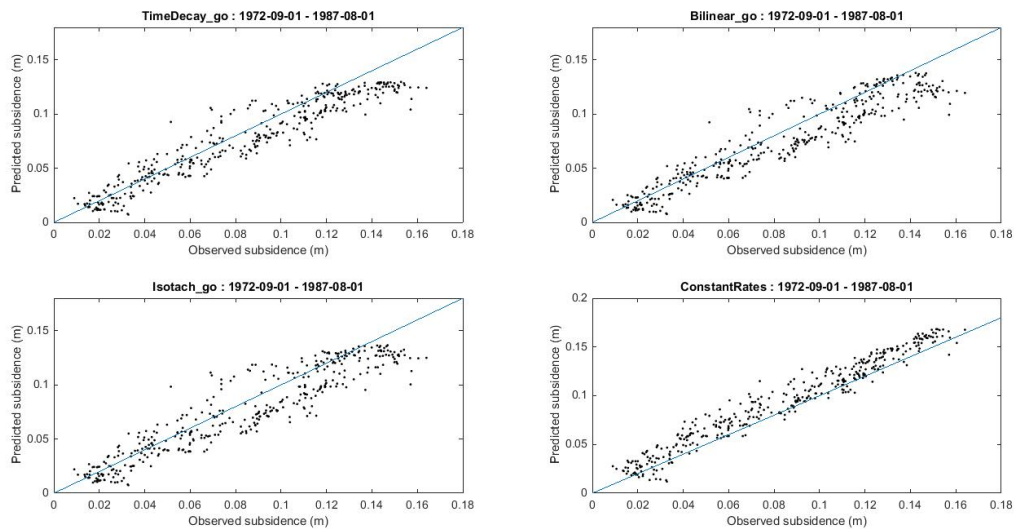
Figure E.3.: Predicted versus measured subsidence for NAM models and a model based on regularised direct inversion to compaction (ConstantRates: see text) for the 1972-09-01 - 1987-08-01 epoch.
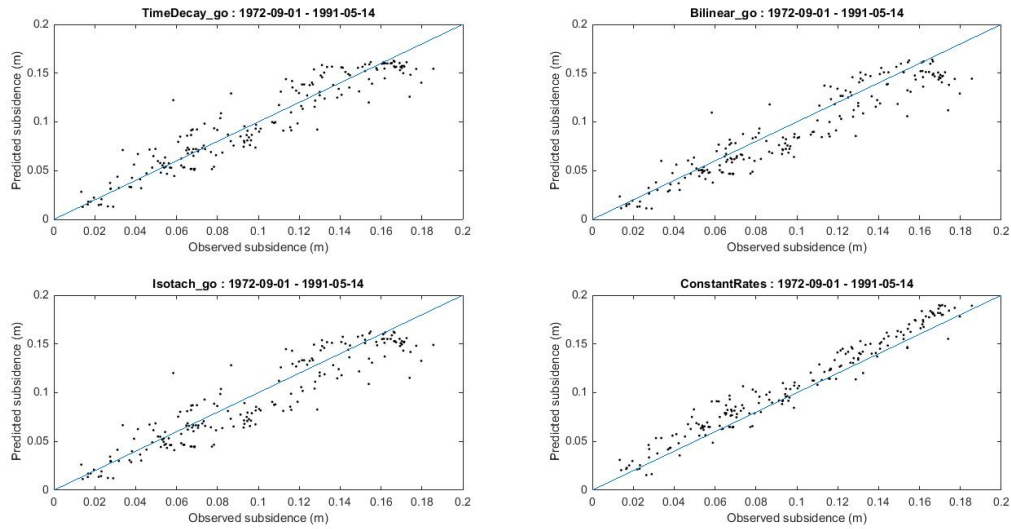
Figure E.4.: Predicted versus measured subsidence for NAM models and a model based on regularised direct inversion to compaction (ConstantRates: see text) for the 1972-09-01 - 1991-05-14 epoch.
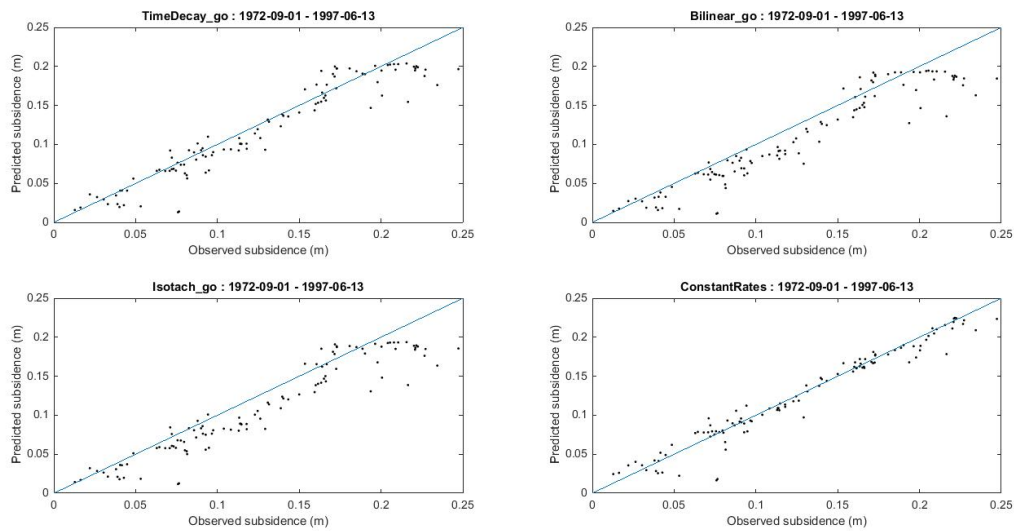
Figure E.5.: Predicted versus measured subsidence for NAM models and a model based on regularised direct inversion to compaction (ConstantRates: see text) for the 1972-09-01 - 1997-06-13 epoch.
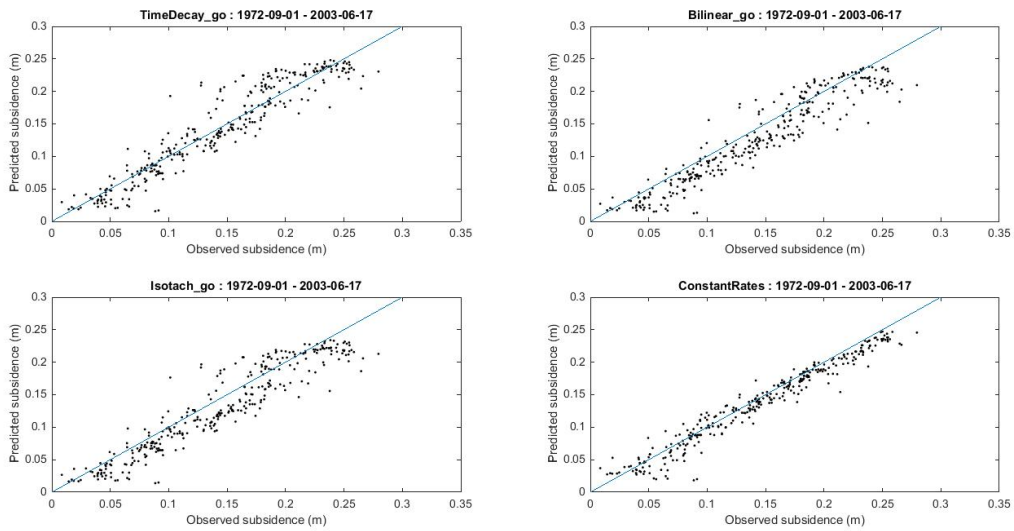
Figure E.6.: Predicted versus measured subsidence for NAM models and a model based on regularised direct inversion to compaction (ConstantRates: see text) for the 1972-09-01 - 2003-06-17 epoch.
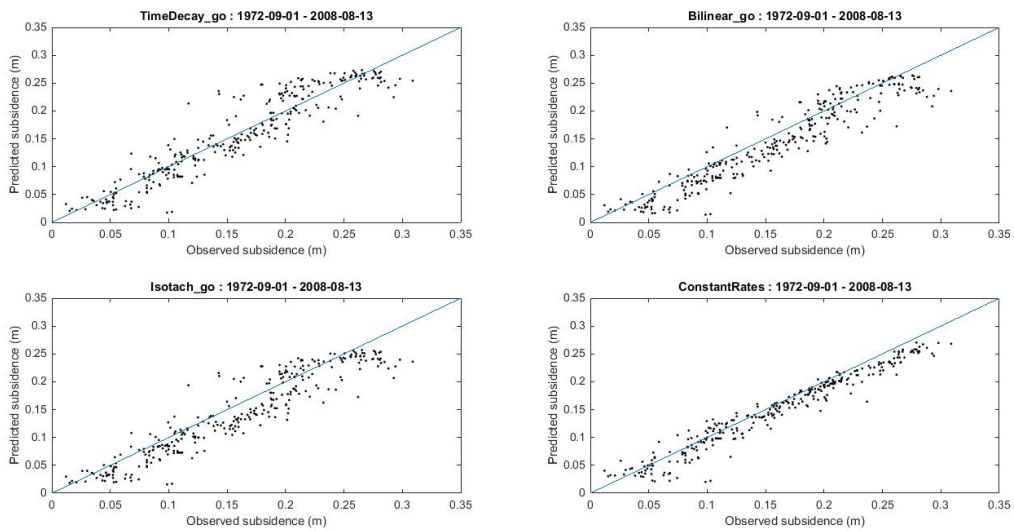
Figure E.7.: Predicted versus measured subsidence for NAM models and a model based on regularised direct inversion to compaction (ConstantRates: see text) for the 1972-09-01 - 2008-08-17 epoch.
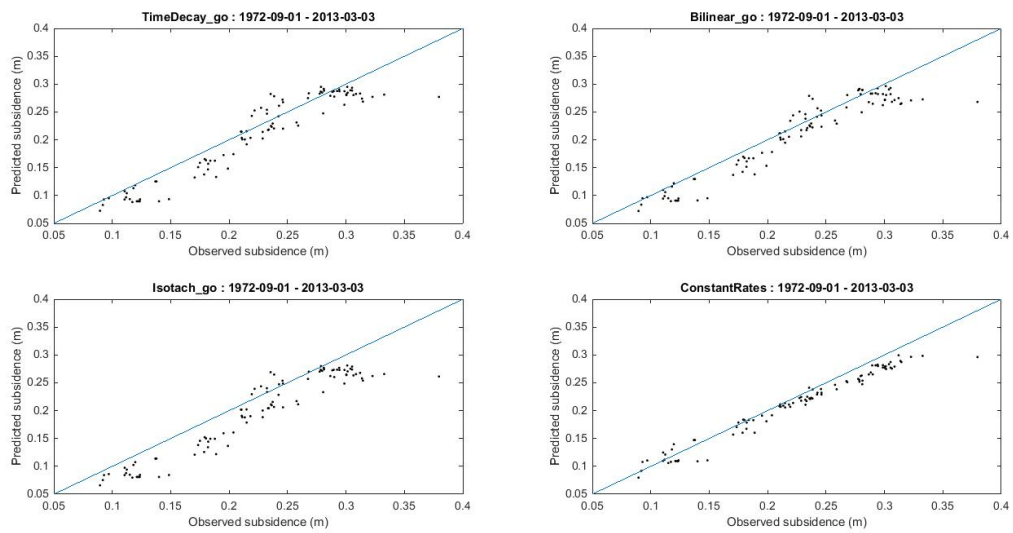
Figure E.8.: Predicted versus measured subsidence for NAM models and a model based on regularised direct inversion to compaction (ConstantRates: see text) for the 1972-09-01 - 2013-03-03 epoch.

References

J Besag, J York, and A Mollie. Bayesian image restoration with application in spatial statistics. *Ann Inst Math Stat*, 43:1–59, 1991.

Arul Earnest, Geoff Morgan, Kerrie Mengersen, Louise Ryan, Richard Summerhayes, and John Beard. Evaluating the effect of neighbourhood weight matrices on smoothing properties of conditional autoregressive (car) models. *International Journal of Health Geographics*, 6(1):54, 2007.

Paul H. C. Eilers and Brian D. Marx. Splines, knots, and penalties. *Wiley Interdisciplinary Reviews: Computational Statistics*, 2(6):637–653, 2010. ISSN 1939-0068.

J. Geertsma and G. Van Opstal. A numerical technique for predicting subsidence above compacting reservoirs, based on the nucleus of strains concept. *Verhandeling Kon. Ned. Geol. Mijnbowk. Gen.*, 26:63–78, 1973.

G. Wahba G.H. Golub, M. Heath. Generalized cross-validation as a method for choosing a good ridge parameter. *Technometrics*, 21(2):215–223, 1979.

T. Hastie, R. Tibshirani, and J. Friedman. *The Elements of Statistical Learning*. Springer-Verlag, 2009.

B. N. Kuvshinov. Elastic and piezoelectric fields due to polyhedral inclusions. *International Journal of Solids and Structures*, 45:1352–1384, 2008.

A Mossop, O van der Wal, and R van Eijs. Subsurface technical report: Subsidence modelling of ameland fields. Technical report, Nederlandse Aardolie Maatschappij, 2011.

A.G. Muntendam-Bos, I.C. Kroon, and P.A. Fokker. Time-dependent inversion of surface subsidence due to dynamic reservoir compaction. *Mathematical Geosciences*, 40(2):159–177, 2008. ISSN 1874-8961.

NAM. Technical addendum to the winningsplan groningen 2013 subsidence, induced earthquakes and seismic hazard analysis in the groningen field. Technical report, NAM, 2013.

M.S. Zhdanov. *Geophysical Inverse Theory and Regularization Problems*. Methods in Geochemistry and Geophysics 36. Elsevier Science B.V., 2002.

Bibliographic information

Classification	Restricted
Report Number	SR.15.11194
Title	Regularised direct inversion to compaction in the Groningen reservoir using measurements from optical leveling campaigns
Subtitle	
Authors	S.M. Bierman (GSNL-PTD/TASE), F. Kraaijeveld (GSNL-PTI/RC), S.J. Bourne (GSNL-PTI/RC)
Keywords	reservoir compaction, Groningen, optical leveling, Rotliegend, inversion
Issue Date	May 2015
Period of work	June 2014 - May 2015
US Export Control	Non US — Public Domain
WBSE Code	ZZPT/015656/010125
Reviewed by	Jonathan, Philip GSUK-PTD/TASE and Park, Timothy A GSUK-PTD/TASE
Approved by	Jonathan, Philip GSUK-PTD/TASE
Sponsoring Company/ Customer	Nederlandse Aardolie Maatschappij B.V.
Spons./Cust. Address	
Issuing Company	Shell Global Solutions International B.V., Amsterdam P.O. Box 38000 1030 BN Amsterdam The Netherlands

Report distribution

Electronic distribution (PDF)

Name, Company, Ref. Ind.
PT Information Services, PTT/TIKE, PT-Information-Services@Shell.com   PDF